

# Myristyl Trimethyl Ammonium Bromide and Octadecyl Trimethyl Ammonium Bromide Are Surface-Active Small Molecule Dynamin Inhibitors that Block Endocytosis Mediated by Dynamin I or Dynamin II<sup>[S]</sup>

Annie Quan, Andrew B. McGeachie, Damien J. Keating, Ellen M. van Dam, Jenny Rusak, Ngoc Chau, Chandra S. Malladi, Chen Chen, Adam McCluskey, Michael A. Cousin, and Phillip J. Robinson

*Cell Signalling Unit, Children's Medical Research Institute, University of Sydney, Sydney, Australia (A.Q., A.B.M., E.M.v.D., J.R., N.C., C.S.M., P.J.R.); Chemistry, School of Environmental and Life Sciences, University of Newcastle, Newcastle, Australia (A.M.); Department of Human Physiology, Flinders University, Adelaide, Australia (D.J.K.), Prince Henry's Institute of Medical Research, Victoria, Australia (C.C.); and, Membrane Biology Group, Centre for Integrative Physiology, University of Edinburgh, Edinburgh, Scotland (M.A.C.)*

Received January 17, 2007; accepted August 16, 2007

## ABSTRACT

Dynamin is a GTPase enzyme involved in membrane constriction and fission during endocytosis. Phospholipid binding via its pleckstrin homology domain maximally stimulates dynamin activity. We developed a series of surface-active small-molecule inhibitors, such as myristyl trimethyl ammonium bromide (MiTMAB) and octadecyltrimethyl ammonium bromide (OcTMAB), and we now show MiTMAB targets the dynamin-phospholipid interaction. MiTMAB inhibited dynamin GTPase activity, with a  $K_i$  of  $940 \pm 25$  nM. It potently inhibited receptor-mediated endocytosis (RME) of transferrin or epidermal growth factor (EGF) in a range of cells without blocking EGF binding, receptor number, or autophos-

phorylation. RME inhibition was rapidly reversed after washout. The rank order of potency for a variety of MiTMAB analogs on RME matched the rank order for dynamin inhibition, suggesting dynamin recruitment to the membrane is a primary cellular target. MiTMAB also inhibited synaptic vesicle endocytosis in rat brain nerve terminals (synaptosomes) without inducing depolarization or morphological defects. Therefore, the drug rapidly and reversibly blocks multiple forms of endocytosis with no acute cellular damage. The unique mechanism of action of MiTMAB provides an important tool to better understand dynamin-mediated membrane trafficking events in a variety of cells.

Endocytosis in eukaryotic cells services the uptake of extracellular material and the recycling of membrane components. Multiple forms of endocytosis exist that regulate a variety of different cellular processes, such as regulation of

cell surface receptor expression and signaling, cell fate determination, cell migration, antigen presentation, and synaptic transmission (Liu and Robinson, 1995; Kaksonen et al., 2006). Two of the best characterized pathways are receptor-mediated endocytosis (RME) and synaptic vesicle endocytosis (SVE). Both use many proteins and lipid-cofactors (Cousin and Robinson, 2001; Le Roy and Wrana, 2005). RME is activated by binding of hormones or growth factor ligands to specific cell surface receptors, for example, transferrin (Tf) and epidermal growth factor (EGF). RME usually occurs via clathrin-coated pits, and it requires the ubiquitously ex-

This work was supported by grants from the National Health and Medical Research Council (Australia) and The Wellcome Trust (Ref. 062841).

Article, publication date, and citation information can be found at <http://molpharm.aspetjournals.org>.  
doi:10.1124/mol.107.034207.

[S] The online version of this article (available at <http://molpharm.aspetjournals.org>) contains supplemental material.

**ABBREVIATIONS:** RME, receptor-mediated endocytosis; SVE, synaptic vesicle endocytosis; Tf, transferrin; EGF, epidermal growth factor; PH domain, pleckstrin homology; PtdIns(4,5)P<sub>2</sub>, phosphatidylinositol-4,5-bisphosphate; MiTMAB, myristyl trimethyl ammonium bromide; OcTMAB, octadecyl trimethyl ammonium bromide; DoTMAB, dodecyl trimethyl ammonium bromide; PS, L-phosphatidylserine; PMSF, phenylmethylsulfonyl fluoride; PFA, paraformaldehyde; FCS, fetal calf serum; DMEM, Dulbecco's modified Eagle's medium; TxR, Texas Red; A, Alexa; DAPI, 4,6-diamidino-2-phenylindole; AM, acetoxymethyl ester; DMSO, dimethyl sulfoxide; GST, glutathione transferase; PSB, phosphate-buffered saline; CI, confidence interval; HRP, horseradish peroxidase; EGFP, enhanced green fluorescent protein; pEGFP, EGFR phosphotyrosine; GFP, green fluorescent protein; PLC, phospholipase C; cmc, critical micellar concentration; WT, wild type; S, stimulation; SV, synaptic vesicle; BAPTA, 1,2-bis(2-aminophenoxy)ethane-*N,N,N',N'*-tetraacetic acid; FM2-10, *N*-(3-triethylammonium propyl)-4-(4-diethylamino)styrylpyridinium dibromide.

pressed GTPase dynamin II (Trowbridge et al., 1993; Le Roy and Wrana, 2005). SVE occurs when nerve terminals retrieve empty synaptic vesicles after stimulated exocytosis to enable refilling of these vesicles with neurotransmitters for a new round of exocytosis. It is mediated by dynamin I. SVE and RME use distinct isoforms of the same proteins, and they have other mechanistic distinctions, for example SVE is stimulated by calcium-dependent activation of the phosphatase calcineurin (Liu and Robinson, 1995; Hinshaw, 2000). Dynamin I, II, and III are all found in neurons, but dynamin I is neuron-specific, and it is expressed at much higher levels than either of the other dynamins (Ferguson et al., 2007).

Dynamin is a 96-kDa GTPase enzyme involved in membrane constriction and fission during RME and SVE. At a late stage of the process, dynamin assembles into rings to form a collar or helix around the neck of the invaginating vesicles. Upon GTP hydrolysis the vesicle is pinched from the plasma membrane (McNiven, 1998) by a conformational twist in the dynamin helix (Roux et al., 2006). Dynamin is also needed for many, but not all, forms of clathrin-independent endocytosis, such as phagocytosis, caveolae internalization, and endocytosis of cytokine receptors in non-neuronal cells, and for fast/rapid endocytosis in neurons and neuroendocrine cells (Artalejo et al., 1997; Hinshaw, 2000; Jockusch et al., 2005). Knockout of the dynamin I gene in mice reveals its central role in SVE, but it also reveals the occurrence of dynamin I-independent SVE at the synapse, presumably mediated by dynamin II or III (Ferguson et al., 2007). Dynamin contains four functional domains: an N-terminal GTPase domain, a pleckstrin homology (PH) domain, a proline-rich domain, and an assembly domain also known as GTPase effector domain (Cousin and Robinson, 2001). Overexpression of GTPase-defective dynamin mutants inhibits both RME and SVE in a variety of cells (Marks et al., 2001). The PH domain of dynamin is relatively nonselective, but it has a small preference for binding phosphatidylinositol-4,5-bisphosphate [PtdIns(4,5)P<sub>2</sub>] (Salim et al., 1996), which enhances its GTPase activity (Lin et al., 1997; Barylko et al., 1998; Vallis et al., 1999) and induces cooperative dynamin helix assembly (Stowell et al., 1999). Deletion of the PH domain elevates the level of dynamin's nonstimulated GTPase activity (Scaife et al., 1998). Therefore, each of dynamins' functional domains is an attractive target for development of dynamin inhibitors, as potential endocytosis inhibitors.

Our aim was to develop dynamin inhibitors as new tools for cell biology and also as potentially clinically useful endocytosis inhibitors. Multiple low-potency and low-specificity endocytosis inhibitors exist: chlorpromazine (Wang et al., 1993; Atwood, 2001), concanavalin A, phenylarsine oxide (Gray et al., 2001), dansylcadaverine (Davies et al., 1984), intracellular potassium depletion (Larkin et al., 1983), intracellular acidification (Lindgren et al., 1997), and decreasing the temperature to 4°C (Wang et al., 1993). Each has poor specificity and low utility, but each nonetheless has contributed significantly to our understanding of endocytosis. We reported previously on the development of long-chain ammonium salts (Hill et al., 2004) and dimeric tyrophostins (Hill et al., 2005) as the first two series of small-molecule inhibitors of the GTPase activity of dynamin.

Two of the most potent inhibitors from the long-chain ammonium salt series of compounds were myristyl trimethyl ammonium bromide (MiTMAB, also known as tetradecyl tri-

methyammonium bromide; CAS no. 1119-97-7) and octadecyltrimethyl ammonium bromide (OcTMAB; CAS no. 1120-02-1). Many pharmacologically active compounds are amphiphilic or hydrophobic molecules whose site of action in an organism is frequently the plasma membrane (Schreier et al., 2000). They tend to self-associate and to interact with biological membranes. Amphiphilic compounds have a long hydrophobic portion and either an ionic (anionic, cationic, or zwitterionic) or a nonionic polar head group. Classes of amphiphilic drugs include phenothiazines, benzodiazepine tranquilizers, analgesics, tricyclic antidepressants, and local anesthetics (Schreier et al., 2000). Trimethyl alkylammonium compounds such as the MiTMAB series have pharmaceutical properties, because they produce long-lasting anesthetic activity that increases with increasing alkyl chain length (Scurlock and Curtis, 1981). In the present study, we report that the mechanism of dynamin inhibition by the MiTMAB series involves a surface activity of the compounds on membranes, and we show that the compounds reversibly inhibit different forms of endocytosis in multiple cell systems.

## Materials and Methods

**Materials.** Phosphatidylserine (PS), phenylmethylsulfonyl fluoride (PMSF), and Tween 80 were from Sigma-Aldrich (St. Louis, MO). GTP was from either Sigma-Aldrich or Roche Applied Science (Mannheim, Germany), and leupeptin was from Bachem (Bubendorf, Switzerland). Gel electrophoresis reagents, equipment, and protein molecular weight markers were from Bio-Rad (Hercules, CA). Collagenase was from Roche. Paraformaldehyde (PFA) was from Merck Pty Ltd. (Kilsyth, Australia). Coverslips were from Lomb Scientific (Sydney, Australia). Penicillin/streptomycin, phosphate-buffered salts, fetal calf serum (FCS), and Dulbecco's modified Eagle's medium (DMEM) were from Invitrogen (Mount Waverley, Victoria, Australia). Texas Red-conjugated transferrin (Tf-TxR), Texas Red-conjugated EGF (EGF-TxR) Alexa-488-conjugated EGF (EGF-A488), Alexa-594-conjugated Tf (Tf-A594), biotinylated-Tf, DAPI, FM2-10, and Fluo-3-AM were from Invitrogen. Unconjugated EGF was from Sigma-Aldrich. All other reagents were of analytical reagent grade or better.

**Drugs.** Drugs were from Sigma-Aldrich. The drugs were made up as stock solutions in 10 to 100% DMSO and diluted in 10% (v/v) DMSO/20 mM Tris-HCl, pH 7.4, before use in the assay. The final DMSO concentration in the GTPase or endocytosis assays was at most 1%. The GTPase assay for dynamin I was unaffected by DMSO up to 1%. MiTMAB was dissolved as 30 mM stocks in 100% DMSO, and it was colorless. Stocks were stored at -20°C for several months. It was diluted into solutions of 10% DMSO (range, 1–10%) made up in 20 mM Tris-HCl, pH 7.4, and then it was diluted again into the final assay.

**Protein Production.** Dynamin I was purified from sheep brain by extraction from the peripheral membrane fraction of whole brain (Robinson et al., 1993) and by affinity purification on GST-Amph2-SH3-Sepharose as described previously (Marks and McMahon, 1998; Quan and Robinson, 2005), yielding 8 to 10 mg of protein from 250 g of sheep brain. Recombinant dynamin I lacking the PH domain (dynamin I-ΔPH; provided by Robin Scaife, Western Australia Institute for Medical Research, Perth, Australia) was expressed in insect cells using baculoviral infection, and it was also affinity-purified on GST-Amph2-SH3-Sepharose beads (Salim et al., 1996).

**Malachite Green GTPase Assay.** The malachite green method was used for the sensitive colorimetric detection of orthophosphate (P<sub>i</sub>). It is based on formation of a phosphomolybdate complex at low pH with basic dyes, causing a color change (Hohenwallner and Wimmer, 1973; Van Veldhoven and Mannaerts, 1987; Geladopoulos et al., 1991). The assay procedure has been described in detail previously,

and it is based on stimulation of native sheep brain-purified dynamin I by sonicated PS liposomes (Quan and Robinson, 2005). However, in our earlier studies, we used 200 nM dynamin I (Hill et al., 2004, 2005; Quan and Robinson, 2005), whereas in the present study we used 20 nM. This slightly reduced the  $IC_{50}$  values for MiTMAB analogs we reported previously (Hill et al., 2004). In brief, purified dynamin I (20 nM) (diluted in dynamin diluting buffer: 6 mM Tris-HCl, 20 mM NaCl, and 0.02% Tween 80, pH 7.5) was incubated in GTPase buffer (10 mM Tris-HCl, 10 mM NaCl, 2 mM  $Mg^{2+}$ , 0.05% Tween 80, pH 7.5, 1  $\mu$ g/ml leupeptin, and 0.1 mM PMSF) and 0.3 mM GTP in the presence of test compound for 30 min at 37°C. The final assay volume was 150  $\mu$ l. The assay was conducted in round-bottomed 96-well plates. The incubations of the plate were performed in a dry heating block with shaking at 300 rpm (Eppendorf Thermomixer; Eppendorf South Pacific, North Ryde, Sydney, Australia). Dynamain activity was measured as phospholipid stimulated with addition of different concentrations of phosphatidylserine liposomes. The reaction was terminated with 10  $\mu$ l of 0.5 M EDTA, pH 8.0, and the samples were stable for several hours at room temperature. To each well, we added 40  $\mu$ l of malachite green solution [2% (w/v) ammonium molybdate tetrahydrate, 0.15% (w/v) malachite green, and 4 M HCl]; the solution was passed through 0.45- $\mu$ m filters, and it was stored in the dark for up to 2 months at room temperature. Color was allowed to develop for 5 min (and it was stable up to 2 h), and the absorbance of samples in each plate was determined on a microplate spectrophotometer at 650 nm [VERSA<sub>max</sub> microplate reader (Molecular Devices, Sunnyvale, CA)]. Phosphate release was quantified by comparison with a standard curve of sodium dihydrogen orthophosphate monohydrate (baked dry at 110°C overnight), which was run in each experiment. GraphPad Prism 4 (GraphPad Software Inc., San Diego, CA) was used for plotting data points and analysis of enzyme kinetics using nonlinear regression. The curves were generated using the Michaelis-Menten equation  $v = V_{max}[S]/(K_m + [S])$ , where S is PS activator or GTP substrate. After the  $V_{max}$  and  $K_m$  values were determined, the data were transformed using the Lineweaver-Burke equation  $1/v = 1/V_{max} + (K_m/V_{max}) \times (1/[S])$ .

**Phospholipid Binding.** Dynamain I (520 nM) purified from whole sheep brain was incubated with PS liposomes (100  $\mu$ M; sonicated into 30 mM Tris-HCl, pH 7.4) in 100  $\mu$ l of assembly buffer [1 mM EGTA, 30 mM Tris, 100 mM NaCl, 1 mM dithiothreitol, 1 mM PMSF, and a Complete protease inhibitor cocktail tablet per 50 ml (Roche Applied Science)] for 30 min at room temperature (22°C). The samples were centrifuged at 14,000g for 15 min to separate lipid-bound and free dynamain, and the fractions were analyzed by gel electrophoresis on a 12% SDS polyacrylamide gel followed by staining with Coomassie Brilliant Blue.

**Texas Red-Tf and Alexa 488-EGF Uptake.** COS-7, HeLa, and A431 cells were cultured in DMEM supplemented with 10% FCS at 37°C in 5% CO<sub>2</sub> in a humidified incubator. Tf and EGF uptake were analyzed based on methods described previously (van der Bliek et al., 1993). In brief, cells were plated on glass coverslips (coated with superfibronectin for A431 cells or poly-D-lysine for COS-7 and HeLa cells) to 60% confluence. The cells were serum-starved overnight (16 h) in DMEM minus FCS. Cells were then incubated with MiTMAB (usually 30  $\mu$ M) or vehicle for 10 or 15 min before addition of 5  $\mu$ g/ml Tf-TxR or 1  $\mu$ g/ml EGF-A488 for 10 or 15 min at 37°C. For washout experiments, this involved one complete change of media (–FCS) after drug treatment and incubation at 37°C for 30 min, after which 600 ng/ml EGF-TxR and 5  $\mu$ g/ml Tf-A594 were added to each well and incubated for 10 or 15 min at 37°C. Cell surface-bound Tf or EGF was removed by incubating the cells in an ice-cold acid wash solution (0.2 M acetic acid and 0.5 M NaCl, pH 2.8) for 15 min. Cells were immediately fixed with 4% PFA for 10 min, and then they were washed three times with PBS. Nuclei were stained using DAPI. Coverslips were mounted using mounting medium containing 1,4-diazabicyclo[2.2.2]octane, and the fluorescence was monitored using a DMLB bright field microscope (Leica Microsystems, Heidelberg,

Germany) and SPOT digital camera (Scitech Pty Ltd, Preston Victoria, Australia).

Quantitative analysis of the inhibition of EGF endocytosis in COS-7 cells was performed on large numbers of cells by an automated process. COS-7 cells were grown in poly-D-lysine-coated 96-well plates, and they were preincubated with varying concentrations of drugs for 15 min before addition of 1  $\mu$ g/ml EGF-A488 for 10 min at 37°C. All conditions were carried out in triplicate. Cells were washed twice with ice-cold PBS, and then they were subjected to an acid wash (0.2 M acetic acid and 0.5 M NaCl, pH 2.8) at 4°C for 10 min to remove surface-bound EGF. Cells were washed again with PBS before fixation in 4% PFA, pH 7.4. Nuclei were stained with DAPI. Green (EGF-A488) and blue (DAPI) images were collected automatically using an Olympus IX81 epifluorescence microscope (Olympus, Sydney, Australia). Nine images were collected from each well, averaging 40 to 50 cells per image. The average integrated intensity of EGF-A488 signal per cell was calculated for each well using MetaMorph (Molecular Devices, Sunnyvale, CA), and the data are expressed as a percentage of control cells (vehicle-treated). The average number of cells for each data point was ~1200.  $IC_{50}$  values were calculated using Prism 4 (GraphPad Software Inc.), and data are expressed as mean  $\pm$  95% confidence interval (CI) for three wells and ~1200 cells.

**Tf and EGF Binding Assays.** For the Tf binding assay,  $1.5 \times 10^5$  COS-7 cells were cultured in six-well culture plates for 2 days, and then the cells were serum-starved for 2 h in DMEM minus FCS. Cells were then incubated with 30  $\mu$ M MiTMAB or DMSO (vehicle control) for 10 min at 37°C, and then they were placed on ice. Biotinylated-Tf (10  $\mu$ g/ml) was then added to cells for the indicated times, and the cells were washed four times with ice-cold PBS. Cells were lysed for 10 min with lysis buffer [20 mM Tris-HCl, pH 7.4, 2 mM EDTA, 2 mM EGTA, 1% Triton X-100, 10  $\mu$ g/ml leupeptin, 1 mM PMSF, Complete protease inhibitor tablet (Roche Applied Science), 2 mM imidazole, 1 mM sodium fluoride, 2 mM sodium orthovanadate, 1 mM sodium molybdate, and 4 mM sodium tartrate dihydrate], centrifuged at 14,000g for 10 min, and the supernatant was harvested as the total cell lysate. Lysates for each condition were resolved on a 10% SDS-polyacrylamide gel and transferred onto Protran immobilized nitrocellulose membrane (PerkinElmer Life and Analytical Sciences, Waltham, MA). The membranes were probed with avidin-conjugated HRP (Invitrogen), and the signal was developed with SuperSignal West Pico chemiluminescence (Pierce Chemical, Rockford, IL). Intensity of the biotinylated-Tf was normalized against an endogenous biotinylated COS-7 cell protein on the same blots, and the range of values ( $n = 2$ ) was plotted.

For the EGF binding assay and microscopy image analysis, A431 cells were grown overnight on 22-mm coverslips coated with 1 ml of 5  $\mu$ g/ml superfibronectin (Sigma-Aldrich). Cells were serum-starved for 2 h, and then they were treated with either DMSO (vehicle control) or 30  $\mu$ M MiTMAB for 10 min at 37°C. Cells were then placed on ice and incubated with 600 ng/ml EGF-A488 for 30 min, fixed in 4% paraformaldehyde, pH 7.5, at RT, and counterstained with DAPI. Images were collected using MetaMorph acquisition software (Molecular Devices), an Olympus IX81 motorized inverted microscope, a Hamamatsu ORCA-ERG (Hamamatsu Photonics, Tokyo, Japan) 12 bit FireWire cooled charge-coupled device camera, and a UPLAPO100 $\times$ OI3 objective (Olympus). Z-stacks were collected at 0.2- $\mu$ m intervals (~70 images/stack), and three-dimensionally deconvoluted using AutoDeblur (AutoQuant Imaging, Inc., Troy, NY). A maximum projection image was then generated. Images are representative of two independent experiments.

**EGFR Activation and Western Blot Analysis.** A431 cells were cultured in 100-mm dishes to 80% confluence, and then the cells were serum-starved overnight (16 h) in DMEM minus FCS. Cells were then incubated with 30  $\mu$ M MiTMAB, DMSO (vehicle control) or 30  $\mu$ M genistein (negative control; Sigma-Aldrich) for 10 min before addition of unconjugated 100 ng/ml EGF for 10 min at 37°C. All conditions were carried out in duplicate. After 10-min incubation,



cells were placed on ice, and then they were washed four times with ice-cold PBS. Total cell lysates were prepared by incubating cells for 10 min with lysis buffer. The mixture was then centrifuged at 14,000g for 10 min, and supernatant was harvested as the total cell lysate. Fifty micrograms of total cell lysate for each condition was resolved on a 12% SDS-polyacrylamide gel, and then it was transferred onto Protran immobilized nitrocellulose membrane (PerkinElmer Life and Analytical Sciences). The membranes were probed with PY20 phosphotyrosine mouse monoclonal antibody (BD Biosciences, San Jose, CA). The secondary antibody was goat anti-mouse polyclonal antibody conjugated to HRP (Dako Denmark A/S, Glostrup, Denmark), and the signal was developed with SuperSignal West Pico chemiluminescence (Pierce Chemical). The membranes were then stripped with 0.2 M NaOH and reprobed for endogenous EGFR using EGFR 1F4 mouse monoclonal antibody (Cell Signaling Technology Inc., Danvers, MA) and developed as described above. Western blots were scanned using a GS800 densitometer (Bio-Rad Laboratories, Hercules, CA), and densitometry analysis was performed by Quantity One software (Bio-Rad Laboratories). EGFR phosphotyrosine (pEGFR) signal was normalized against total EGFR signal, and it was expressed as relative intensity (percentage) of the stimulated control (DMSO) condition and the average of range of values ( $n = 2$ ) was plotted.

**PH Domain Localization in Cells.** The cDNA of the PH domain of dynamin I (rat sequence, amino acids Thr-511 to Lys-635) was cloned by PCR and recombination into the Gateway entry vector pDONR201 (Invitrogen). The cDNA was subcloned by recombination into pcDNA-DEST53 (mammalian N-terminal GFP-tag) expression vector (Invitrogen). HeLa or COS-7 cells were plated on glass coverslips, and then they were transfected with 0.2  $\mu$ g of GFP-dyn I-PH or GFP-PLC $\delta$ -PH DNA per well (24 wells/550  $\mu$ l final volume/well) using FuGENE (Roche Diagnostics) according to the manufacturer's instructions and analyzed 48 h after transfection. Cells were serum-starved for 2 h at 37°C after which they were treated with 30  $\mu$ M MitMAB or 30  $\mu$ M myristic acid for 10 min, and then they were incubated a further 20 min in the presence of Tf-A594 or EGF-TxR as an internal positive controls that the drugs worked and that the DNA construct was not inhibitory (Supplemental Figure S1). Cells were then fixed with 3% PFA in PBS. The distribution of GFP-dyn I-PH, GFP-PLC $\delta$ -PH, and Tf-A594 or EGF-TxR was determined by fluorescence microscopy in the green and red channels, respectively. Optical sections were analyzed by confocal laser scanning microscopy using a TCS SP2 system (Leica Microsystems).

**Chromaffin Cells, Carbon Fiber Amperometry, and Ca<sup>2+</sup> Imaging.** Adult male Wistar rats were killed by carbon dioxide inhalation as approved by the Monash Medical Centre Animal Care Committee. Adrenal glands (four–six) were dissected in ice-cold Ca<sup>2+</sup>-free Locke's buffer consisting of 154 mM NaCl, 5.6 mM KCl, 3.6 mM NaHCO<sub>3</sub>, 5.6 mM glucose, and 5.0 mM HEPES, pH 7.4, and then they were incubated with 3 mg/ml collagenase type A in Locke's buffer in a shaking bath at 37°C for 15, 10, and 5 min with trituration between incubations. After centrifugation at 400g for 5 min, cells were resuspended in DMEM supplemented with 1% penicillin/streptomycin and 10% FCS, filtered through a nylon mesh, centrifuged at 400g for 5 min, plated on 35-mm culture dishes, and incubated at 37°C with 10% CO<sub>2</sub>. Cells were maintained in primary culture for 5 to 7 days before experiments to maximize their secretory capacity. Catecholamine release from single chromaffin cells was measured using carbon fiber amperometry as described previously (Chow et al., 1992). A voltage of +800 mV was applied under voltage-clamp conditions to a carbon fiber electrode (ProCFE; Dagan, Minneapolis, MN) on an individual chromaffin cell. The current due to catecholamine oxidation was recorded with an EPC-9 amplifier and Pulse software (HEKA Electronic, Lambrecht/Pfalz, Germany), sampled at 10 kHz, and low-pass filtered at 1 kHz. Secretory events were analyzed (Mini Analysis version 6.0.1; Synaptosoft, Decatur, GA) for a period of 1 min from the start of exposure to the high-KCl-containing (70 mM KCl replaced an equimolar amount of NaCl) bath

solution. When MitMAB- or DMSO-containing solution was applied, secretory events were analyzed for 10 min. Standard bath solution contained 140 mM NaCl, 5 mM KCl, 2 mM CaCl<sub>2</sub>, 1 mM MgCl<sub>2</sub>, 5 mM D-glucose, and 10 mM HEPES, pH 7.4. Both control and high-KCl solutions were applied to cells using a gravity perfusion system, the outlet of which was within 500  $\mu$ m of the recorded cell. All experiments were carried out at room temperature (22–24°C). After the first stimulation, cells were continuously washed in control bath solution for 5 min to allow them to recover, and then a solution containing either 30  $\mu$ M MitMAB (from a stock of 10 mM in DMSO) or an equivalent volume of DMSO alone (control) was continuously applied to cells for 10 min at room temperature. Cells were stimulated a second time with high-KCl solution. For single cell Ca<sup>2+</sup> imaging, cells were loaded with the Ca<sup>2+</sup> indicator Fluo-3-AM at 5  $\mu$ M in serum-free DMEM at 37°C for 45 min. Before the recording, the cells were rinsed with and kept for at least 10 min in bath solution to allow for full de-esterification of the dye. The cells were perfused at 2 ml/min. Confocal microscopy was applied using an argon ion laser (Olympus) scanning at a peak of 488 nm, and emitted light was detected at wavelengths >515 nm. Images were captured and analyzed using supplied software (Fluoview-300; Olympus). Laser intensity was reduced to 5% of maximum by use of neutral density filters, and the scan rates were kept at 1 scan per 5 s to avoid photobleaching. Changes in intracellular Ca<sup>2+</sup> levels were taken as the ratio of the maximum mean pixel value of the whole cell during stimulation compared with that in the control period to rule out the influence of cell batch or Fluo-3 loading efficiencies (Keating et al., 2001). This ratio is calculated according to the equation  $R = (F - F_{\min})/F_{\min}$ , where  $R$  is the ratio of fluorescence change,  $F_{\min}$  is mean fluorescence intensity during control period, and  $F$  is maximum fluorescence intensity during stimulation. All results were normalized to the response to high KCl under control conditions, which was assigned a value of 1. All data are displayed as mean  $\pm$  S.E.M., and data were tested for significant differences using one-way analysis of variance for comparisons between groups and Student's paired  $t$  test for comparisons within groups.  $p < 0.05$  was set as the limit for statistical significance.

**Endocytosis and Exocytosis in Synaptosomes.** Both assays were performed in rat brain Percoll-purified synaptosomes (Dunkley et al., 1986) as described previously using FM2-10 uptake to measure endocytosis (Cousin and Robinson, 1998; Cousin and Robinson, 2000) or enzyme-linked fluorescent detection of released glutamate (Nicholls and Sihra, 1986; Cousin and Robinson, 2000). Synaptosomes were incubated with either plus (118.5 mM NaCl, 4.7 mM KCl, 1.18 mM MgCl<sub>2</sub>, 1.3 mM CaCl<sub>2</sub>, 0.1 mM K<sub>2</sub>HPO<sub>4</sub>, 20 mM HEPES, and 10 mM glucose, pH 7.4) or minus (1 mM EGTA, no CaCl<sub>2</sub>) Krebs-like medium supplemented with 30  $\mu$ M MitMAB for 10 min before stimulation with 30 mM KCl where indicated.

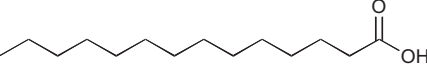
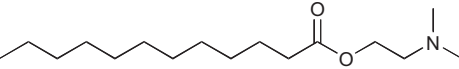
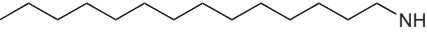
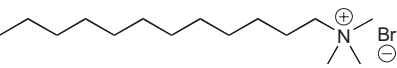
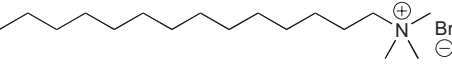
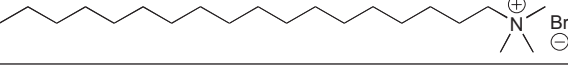
**Electron Microscope.** Purified synaptosomes were incubated for 5 min in Krebs-like medium containing 1.2 mM Ca<sup>2+</sup>, then stimulated with 41 mM KCl for 2 min at 37°C. Synaptosomes were either untreated or preincubated with 30  $\mu$ M MitMAB 5 min before KCl addition. After stimulation, synaptosomes were pelleted in a microfuge at 14,000g for 2 min at room temperature, then fixed by gentle resuspension in Krebs-like medium supplemented with 5% glutaraldehyde for 1 h at 4°C. Synaptosome pellets were gently washed three times with Krebs buffer with low spins (2350g) for 7 min, then gently resuspended in a 10% bovine serum albumin in H<sub>2</sub>O for 20 min at room temperature. The synaptosomes were then recentrifuged at low speed, overlaid with fixative (1% glutaraldehyde in Krebs-like medium), and incubated at 4°C overnight. The pellets were rinsed, stained in a buffered solution of osmium tetroxide for 3 h, rinsed, and incubated for 1 h in 2% aqueous uranyl acetate. Samples were dried by a series of sequential 10-min washes: 50% ethanol and 0.1% NaCl, 70% ethanol and 0.1% NaCl, 95% ethanol and 0.1% NaCl, 100% ethanol and 0.1% NaCl twice, and 100% acetone twice. The synaptosomes were infiltrated with an acetone/

resin mixture (1:1) for 1 h, washed three times for 10 min in Spur's epoxy resin at 70°C, and then embedded within conical shaped molds filled with Spur's epoxy resin for 10 h at 70°C. An ultramicrotome Ultracut-E (Reichert-Jung, Heidelberg, Germany) was used to obtain 0.08- $\mu$ m epoxy sections from the resin blocks. The sections were cut with a diamond knife (Diatome, Biel, Switzerland), floated on water drops, placed on electron microscopy grids, and double stained, first using 2% uranyl acetate in ethanol for 15 min, and then in Reynold's lead citrate for 4 min. The grids were washed in water, touch-dried using absorbent filter paper, and stored until analysis with an electron microscope. Analysis was performed on a 1L-BioTwin electron microscope (Philips, Eindhoven, The Netherlands), and pictures were printed on electron microscope plate film (4489; 8.3  $\times$  10.2 cm; Eastman Kodak, Rochester, NY).

## Results

**MiTMAB Inhibited the GTPase Activity of Dynamain I.** MiTMAB is a 14-carbon alkyl chain with a trimethylated ammonium head group and a bromide counter ion (Table 1, entry 5) reported previously to inhibit dynamain I GTPase activity ( $IC_{50}$  of  $5.79 \pm 2.06 \mu$ M) (Hill et al., 2004). In the present study, the GTPase assay was redesigned to use lower dynamain concentrations (20 nM instead of 200 nM), and the activity of a number of other long-chain amines and ammonium salts (MiTMAB analogs) was reassessed (Table 1). The new  $IC_{50}$  for MiTMAB was little changed ( $3.1 \pm 0.2 \mu$ M; Table 1). The full concentration-response curve is shown in Fig. 1A. When the alkyl chain length was increased to 18 carbons (OcTMAB), the potency increased to  $1.9 \pm 0.2 \mu$ M, and when the chain length was decreased to the dodecyl form, potency dropped to  $9.0 \pm 1.4 \mu$ M (Table 1). The simpler fatty amine salt analogs of these cationic amphiphiles were also examined. Replacing the trimethyl bromide head with an amine or dimethyl amino group produced  $IC_{50}$  values of  $6.5 \pm 1.0$  and  $9.2 \pm 0.96 \mu$ M, respectively (Table 1). The acid form of MiTMAB, myristic acid, was inactive. Therefore, a diverse range of cationic amphiphiles exhibits a tight structure-activity relationship toward dynamain I.

TABLE 1  
Inhibition of dynamain I GTPase activity by long-chain acids, amines, and ammonium salts

| Compound                             | Structure  | Mol. Wt. | $IC_{50}$<br>$\mu$ M |
|--------------------------------------|--|----------|----------------------|
| 1 Myristic acid                      |  | 228.4    | >300                 |
| 2 2-(Dimethyl amino) ethyl myristate |  | 299.5    | $9.2 \pm 0.96$       |
| 3 Tetradecylamine                    |  | 213.4    | $6.5 \pm 1.0$        |
| 4 DoTMAB                             |   | 308.4    | $9.0 \pm 1.4$        |
| 5 MiTMAB                             |  | 336.4    | $3.1 \pm 0.2$        |
| 6 OcTMAB                             |  | 392.5    | $1.9 \pm 0.24$       |

**MiTMAB Targeted the Dynamain I-Phospholipid Interaction.** PS or PtdIns(4,5) $P_2$  binds the PH domain of dynamain, enhances its GTPase activity (Zheng et al., 1996; Lin et al., 1997), and induces cooperative helix assembly (Stowell et al., 1999). The dynamain I GTPase assay used PS liposomes to maximally activate dynamain I. The MiTMAB series of compounds are surface-active, and they are predicted to alter protein-lipid interactions (Scurlock and Curtis, 1981; Schreier et al., 2000). At high concentrations [at, or exceeding, the critical micellar concentration (cmc); see *Discussion*], these compounds are cationic surfactants, as observed for other pharmacologically active cationic amphiphilic compounds such as chlorpromazine or imipramine (Ahyayauch et al., 2002). Therefore, several approaches were used to determine whether MiTMAB targets the dynamain-phospholipid interaction. First, the effect of MiTMAB on the GTPase activity of full-length wild-type (WT) dynamain I purified from sheep brain was compared with that of a recombinant dynamain I lacking the PH domain, dynamain I- $\Delta$ PH (Scaife et al., 1998). WT dynamain I GTPase activity was stimulated by PS liposomes (1.2  $\mu$ M), and it was inhibited by MiTMAB (10 and 30  $\mu$ M) (Fig. 1B). In contrast, dynamain I- $\Delta$ PH was constitutively active, and its activity was unaffected by further PS addition (Fig. 1C), as reported previously (Scaife et al., 1998; Vallis et al., 1999). The GTPase activity of dynamain I- $\Delta$ PH was insensitive to MiTMAB (10 or 30  $\mu$ M; Fig. 1C). This reveals that MiTMAB inhibits the liposome-stimulated dynamain I GTPase activity by targeting the dynamain-phospholipid interaction.

The second approach examined dynamain I binding to liposomes using a sedimentation assay. In this assay, dynamain and liposomes are coincubated and the extent of their interaction is revealed by sedimentation of dynamain by centrifugation. This is a dynamain-phospholipid interaction effect, because mutations in the PH domain that block phospholipid interaction are known to arrest dynamain sedimentation (Vallis et al., 1999). Dynamain alone (520 nM) did not sediment in

this assay; it remained largely in the supernatant (Fig. 1D, lanes 1 and 2), but in the presence of liposomes (100  $\mu$ M), it was found in the pellet (lanes 3 and 4). Phospholipid binding was unaffected by the vehicle control DMSO (lanes 5 and 6); however, MiTMAB reduced lipid binding in a concentration-dependent manner (lanes 7–16). There was a 50% block in dynamin sedimentation at 100  $\mu$ M MiTMAB. The apparent decrease in potency compared with the  $IC_{50}$  in the GTPase assay is probably due to the much higher dynamin and liposome concentrations used in this assay. In addition, MiTMAB does not affect dynamin self-assembly in a sedimentation assay (data not shown). The result suggests MiTMAB prevents dynamin association with phospholipids but not dynamin oligomerization.

The third approach was to investigate the kinetics of dynamin's GTPase activity in the presence of different concentrations of liposomes or GTP. Kinetic analysis using increasing concentrations of GTP revealed the maximal velocity of

dynamin I GTPase activity,  $V_{max}$ , was  $430 \pm 57$  nmol/mg/min, and the Michaelis-Menten constant,  $K_m$ , was  $20.9 \pm 10$   $\mu$ M. In the presence of MiTMAB, the  $V_{max}$  decreased and  $K_m$  increased with increasing concentrations of the drug (data not shown). The Lineweaver-Burke plot shows noncompetitive inhibition with respect to GTP (Fig. 2, A and B). Therefore, MiTMAB does not compete with GTP for binding to the GTPase domain of dynamin. Using increasing concentrations of PS, the  $V_{max}$  was  $427 \pm 40$  nmol/mg/min, and the  $K_m$  was  $3.1 \pm 0.9$   $\mu$ M (Fig. 2, C–E). Lineweaver-Burke double reciprocal plots indicated competitive inhibition with PS (Fig. 2D). In the presence of MiTMAB, there was no effect on  $V_{max}$ , but there was an increased  $K_m$  (data not shown). This indicates MiTMAB is a competitive inhibitor with respect to PS with an inhibition constant,  $K_i$ , of  $940 \pm 25$  nM (Fig. 2E). All together, these data show that MiTMAB is a surface-active compound that competes for PS binding to the dynamin I PH domain.

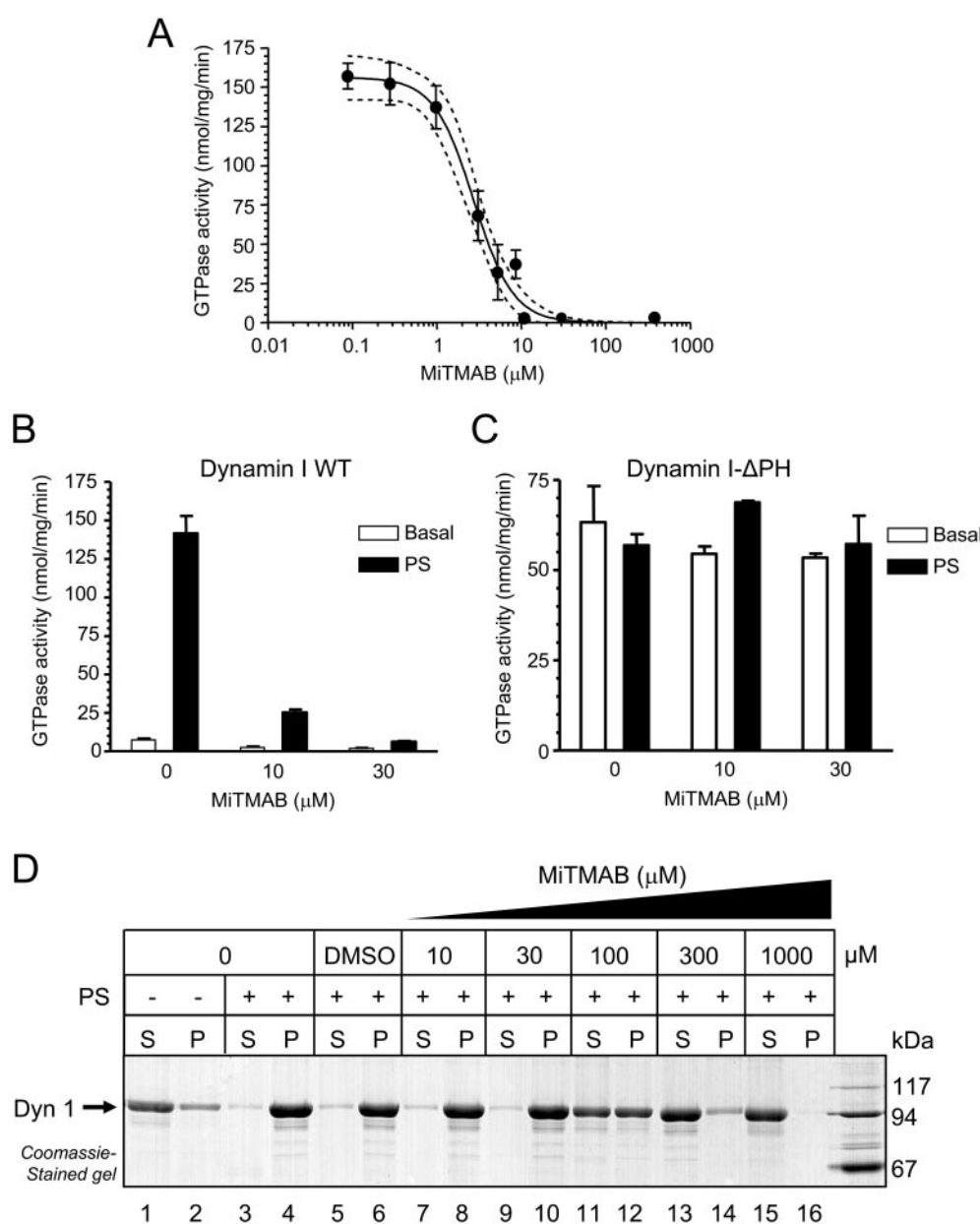


**Fig. 1.** MiTMAB inhibits the GTPase activity of dynamin I and targets the PH domain. **A**, GTPase activity of native sheep brain dynamin I (20 nM) was determined in the presence of different concentrations of MiTMAB. PS (1.2  $\mu$ M)-stimulated activity (filled symbols) was measured. The graph is representative of three independent experiments. Results are mean (triplicates) with a 95% CI (dashed line) for each experiment. **B** and **C**, effect of MiTMAB on basal and PS (1.2  $\mu$ M)-stimulated dynamin I (WT; **B**) and dynamin I- $\Delta$ PH (**C**) GTPase activity was compared in the absence or presence of 10 and 30  $\mu$ M MiTMAB. The values are the means  $\pm$  S.E.M.,  $n = 3$ . Although WT and  $\Delta$ PH dynamin were both used at 20 nM in this assay, the maximal activity of  $\Delta$ PH was approximately half that of WT, because the recombinant  $\Delta$ PH lacks the cooperative lipid-mediated assembly enhanced GTPase activity. **D**, in vitro phospholipid binding; WT dynamin was incubated with phospholipid in the absence and presence of MiTMAB at the concentrations indicated. The Coomassie-stained polyacrylamide gel is a representative image of three independent experiments with similar results. S, supernatant; P, pellet.



**MiTMAB Blocked RME in Non-Neuronal Cells.** Dynamin II is essential for RME, because dominant-negative mutations in its GTPase domain that cause defects in GTP binding or ablation of its GTPase activity result in arrest of Tf uptake in non-neuronal cells (Koenig and Ikeda, 1989; Damke et al., 2001). We next determined the effect of MiTMAB on this dynamin II-dependent process in different non-neuronal cell lines. We examined the effect of MiTMAB on Tf and EGF internalization in HeLa (Fig. 3), HER14, A431, and COS-7 cells (data not shown). Tf and EGF are both internalized by RME, although they traffic to different subcellular compartments after internalization (Sheff et al., 2002; Gáborik and Hunyady, 2004). After 15 min of internalization under control conditions (DMSO treatment), the cells showed considerable staining of Tf-TxR (Fig. 3, A and C) in the periphery and perinuclear region of the cell, which is typical

of Tf localization in early and recycling endosomes (Sheff et al., 2002; Gáborik and Hunyady, 2004). The same cells showed punctate intracellular staining of EGF-A488 (Fig. 3, B and C) in the perinuclear region, typical of EGF internalization to late endosomes and lysosomes. After 10-min preincubation, 30  $\mu$ M MiTMAB reduced RME of Tf (Fig. 3D) and EGF (Fig. 3E), and internalization was completely blocked at 100  $\mu$ M (Fig. 3, G and H). Note that cell morphology was unaffected by the drug treatment (Fig. 3I), even after 30 min of exposure (data not shown), indicating that there was no membrane disruption. The results were confirmed in two other cell lines (data not shown; also see below for COS-7 cells). Therefore, MiTMAB effectively blocks RME of Tf and EGF into non-neuronal cells.

To determine whether the effects of MiTMAB are reversible, we examined the recovery of RME in A431 cells after an

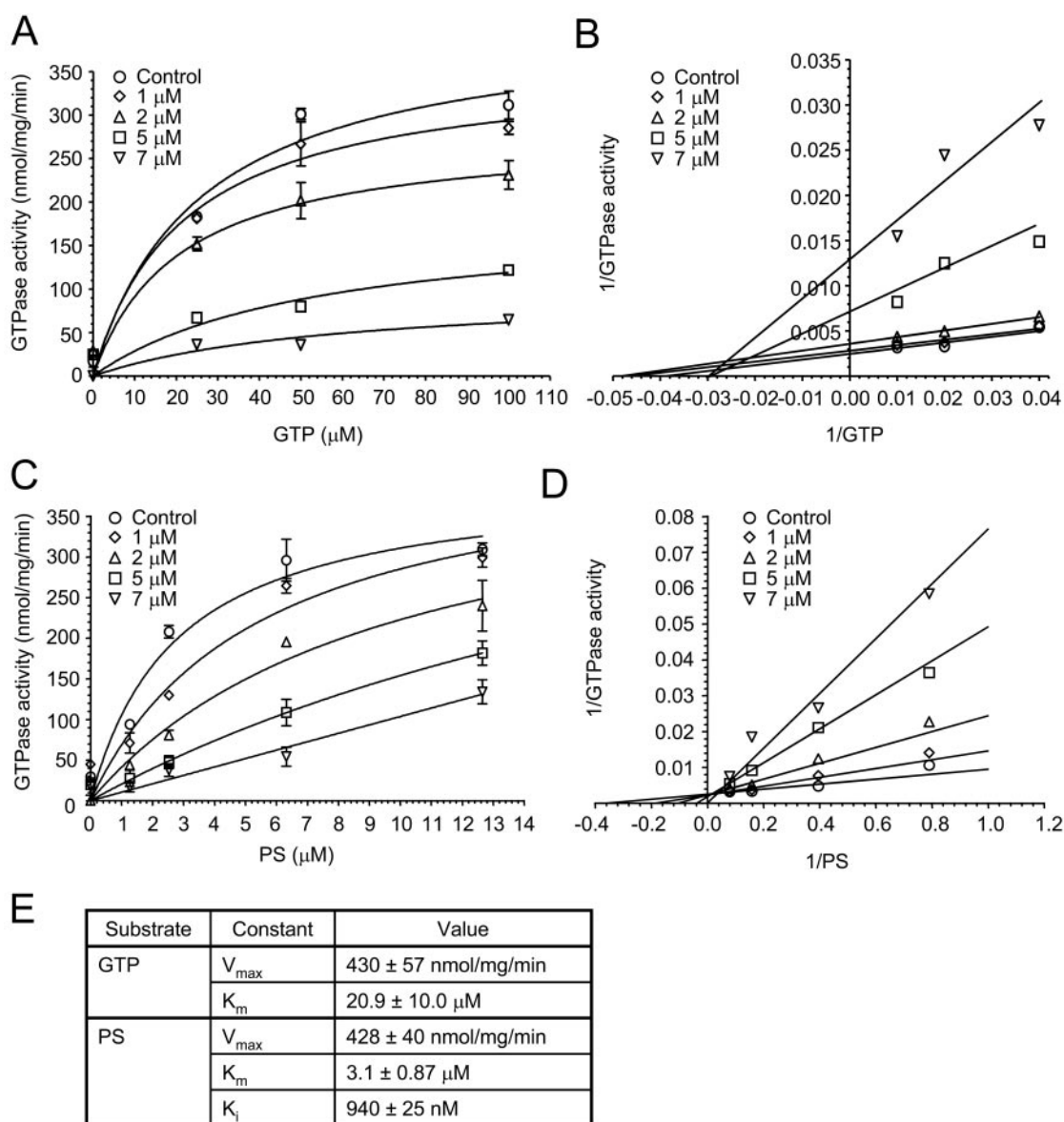


**Fig. 2.** MiTMAB is a competitive inhibitor with PS and noncompetitive with GTP. The effect of MiTMAB on Michaelis-Menten (A) and Lineweaver-Burke (B) plots of the GTPase activity of WT dynamin I (20 nM) with increasing concentrations of GTP and a fixed concentration of PS (12.7  $\mu$ M). Michaelis-Menten (C) and Lineweaver-Burke (D) plots of the GTPase activity of WT dynamin I in the absence and presence of indicated concentrations of MiTMAB at increasing concentrations of PS liposomes and a fixed concentration of GTP (300  $\mu$ M). E, Michaelis-Menten constants  $V_{max}$ ,  $K_m$ , and  $K_i$  with a 95% CI were calculated from triplicate samples performed during a single experiment. All results are representative of at least two independent experiments.

endocytic block with MiTMAB followed by drug washout. EGF endocytosis was greatly reduced in A431 cells incubated with MiTMAB (30  $\mu$ M for 10 min) (Fig. 3, J–K). When endocytosis was measured 30 min after washout of MiTMAB, it was found to have returned to control levels (Fig. 3L). The same results were obtained in these cells for RME of Tf (data not shown). Therefore, the effects of MiTMAB in cells are reversible 30 min after treatment. The same results were obtained after only a 5-min washout (data not shown), suggesting MiTMAB is a rapidly reversible inhibitor.

To quantify the effect of MiTMAB in COS-7 cells, we established an automated quantitative RME assay based on endocytosis of EGF-A488. The  $IC_{50}$  for inhibition of RME by MiTMAB in COS-7 cells was  $20.9 \pm 3.2$   $\mu$ M (Fig. 3, M and N), which compares favorably with the  $IC_{50}$  for dynamin inhibition in vitro. OcTMAB was slightly more potent, DoTMAB was 8-fold less potent, and tetradecylamine was 2-fold less potent (Fig. 3, M–P). 2-(Dimethylamino) ethyl myristate and myristic acid were both without effect. This rank order of potency for RME inhibition closely matches the rank order of

potency for inhibition of the GTPase activity of dynamin (Table 1), suggesting that the mechanism of inhibition is via dynamin. As expected, the ester derivative of myristic acid, 2-(dimethylamino) ethyl myristate, had almost no cellular activity, despite good in vitro potency. This compound was designed as a prodrug to be rapidly cleaved to myristic acid (which is inactive) and dimethylamino ethanol by endogenous intracellular esterases.

**MiTMAB Did Not Block Tf or EGF Binding or EGFR Activation.** To determine that the effect of MiTMAB on RME is intracellular and is not due to blocking initial ligand binding to its receptor, we examined its effect on Tf and EGF binding to their respective cell surface receptors. It is well known that these ligands bind to their receptors on the cell surface in ice-cold conditions but are not internalized. Therefore, we examined the effect of MiTMAB on cell surface binding of 10  $\mu$ g/ml biotinylated-Tf to COS-7 cells in ice-cold conditions, and we measured the amount of Tf binding using Western blot analysis and densitometry. Tf binding was detected at relatively high levels 1 min after addition of Tf in

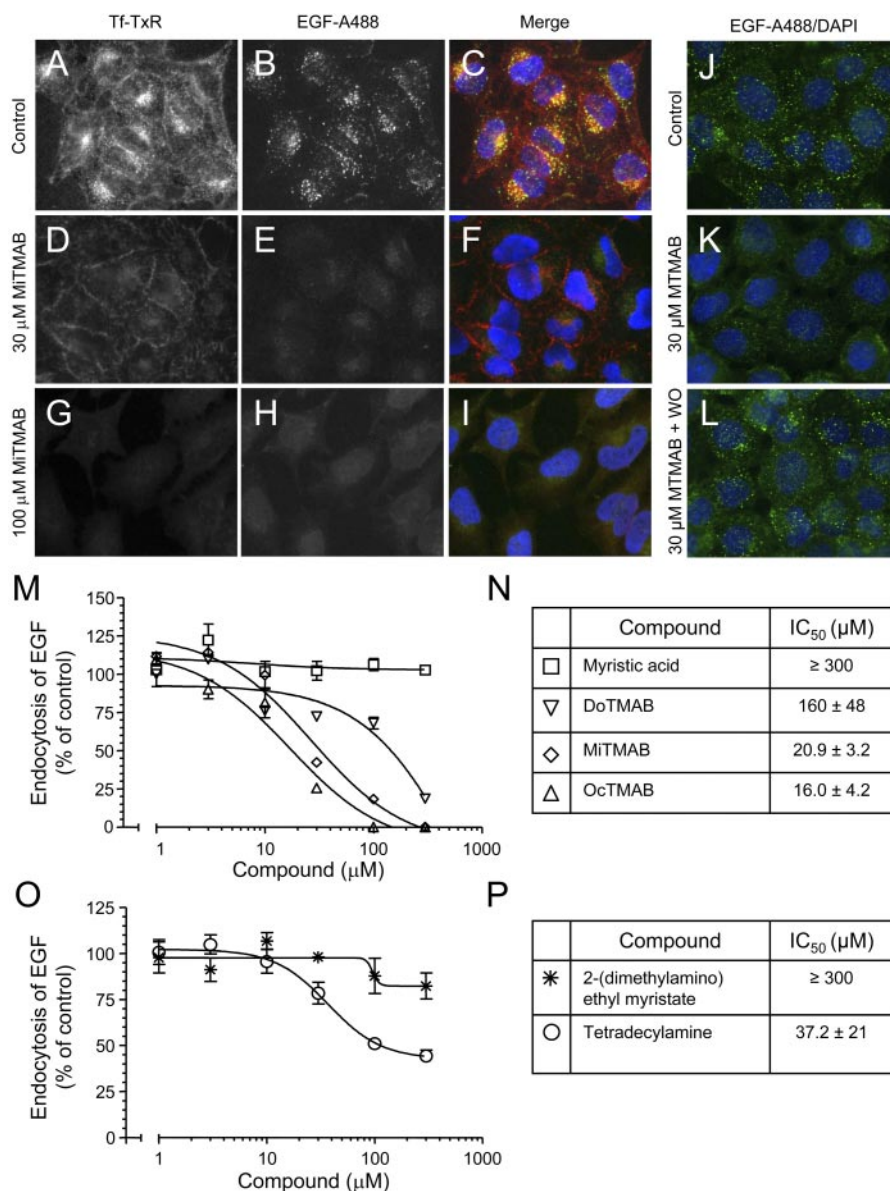


**Fig. 3.** MiTMAB blocks internalization of Tf-TxR and EGF-A488 in non-neuronal cells. HeLa cells were preincubated with vehicle only (A–C) or MiTMAB (D–F; 30 or 100  $\mu$ M) for 10 min. Cells were then incubated with Tf-TxR (A, D, and G) and EGF-A488 (B, E, and H) for 15 min at 37°C, acid-washed, and fixed, and then internalized Tf-TxR and EGF-A488 was detected by fluorescence microscopy. Nuclei were stained blue with DAPI to show the position of the cells (C, F, and I). J to L, MiTMAB is a reversible inhibitor. A431 cells were preincubated with vehicle only (J) or 30  $\mu$ M MiTMAB (K and L) for 10 min, and then they were incubated with EGF-A488 for 10 min. Cells treated as described in K were washed for 30 min without MiTMAB, and then they were incubated with EGF-A488 for 10 min. Images are representative of two independent experiments. M and O, quantitative analysis of EGF-A488 endocytosis in COS-7 cells in the presence of different concentrations of the inhibitors. Data are mean fluorescence as a percentage of fluorescence in control cells (triplicate determinations on approximately 1200 cells each)  $\pm$  S.E.M. The results are representative of three independent experiments. Endocytosis in control cells (no drug, DMSO-treated) is expressed as 100%. N and P,  $IC_{50}$  values  $\pm$  95% CI for the data in M and O, respectively.



both control (vehicle only) and 30  $\mu$ M MiTMAB-treated cells (Fig. 4A). Tf binding was maximal within 5 min, and maximal binding was not altered in MiTMAB-treated cells. Therefore, MiTMAB does not interfere with Tf binding to cell surface receptors.

To search for potential effects of MiTMAB on EGF binding to the EGFR, we used deconvolution fluorescence microscopy to detect total surface binding in Z-stack images. Because of the low levels of EGFR in many cell types and difficulties to isolate detectable levels of the EGFR in cell lysates, we used A431 human carcinoma cells, because they overexpress the endogenous EGFR due to genomic amplification. In vehicle-treated control cells, EGF-A488 bound to the cell surface, and it was not internalized at 4°C (Fig. 4, B and C; Supplemental Movie S1). In cells treated with 30  $\mu$ M MiTMAB for 10 min, the total amount of binding of EGF-A488 to the cell surface was unchanged. However, distribution of the cell surface binding was altered by MiTMAB treatment, resulting in increased localization of the EGFR at cell-cell contacts (Fig. 4, D and E; Supplemental Movie S2). MiTMAB was also without effect on total cellular expression levels of the EGFR (Fig. 4F). Together, this suggests that MiTMAB produces

moderate redistribution of the EGFR but that it does not alter total receptor levels.

By measuring receptor autophosphorylation on tyrosine residues, we next asked whether MiTMAB inhibits EGFR activation. A431 cells stimulated with 100 ng/ml EGF for 10 min had increased EGFR autophosphorylation (Fig. 4, F and G). Both MiTMAB and OcTMAB were without effect. In contrast, genistein (a known protein tyrosine kinase inhibitor that inhibits EGFR autophosphorylation) at 30  $\mu$ M for 10 min abolished EGF-stimulated autophosphorylation. Therefore, MiTMAB and OcTMAB do not seem to inhibit RME via effects on signaling from the activated EGFR.

**MiTMAB Blocked PH Domain Localization to the Plasma Membrane.** Dynamins associates with the plasma membrane via its PH domain interaction with the membrane phospholipids. Mutations in the dynamin PH domain block RME (Achiriloaie et al., 1999). To correlate the in vitro observations that MiTMAB blocks the dynamin-phospholipid interaction and to determine whether MiTMAB targets dynamin localization to the plasma membrane during RME, HeLa cells were transfected with a GFP-dyn I-PH construct to examine its membrane association in cells using confocal

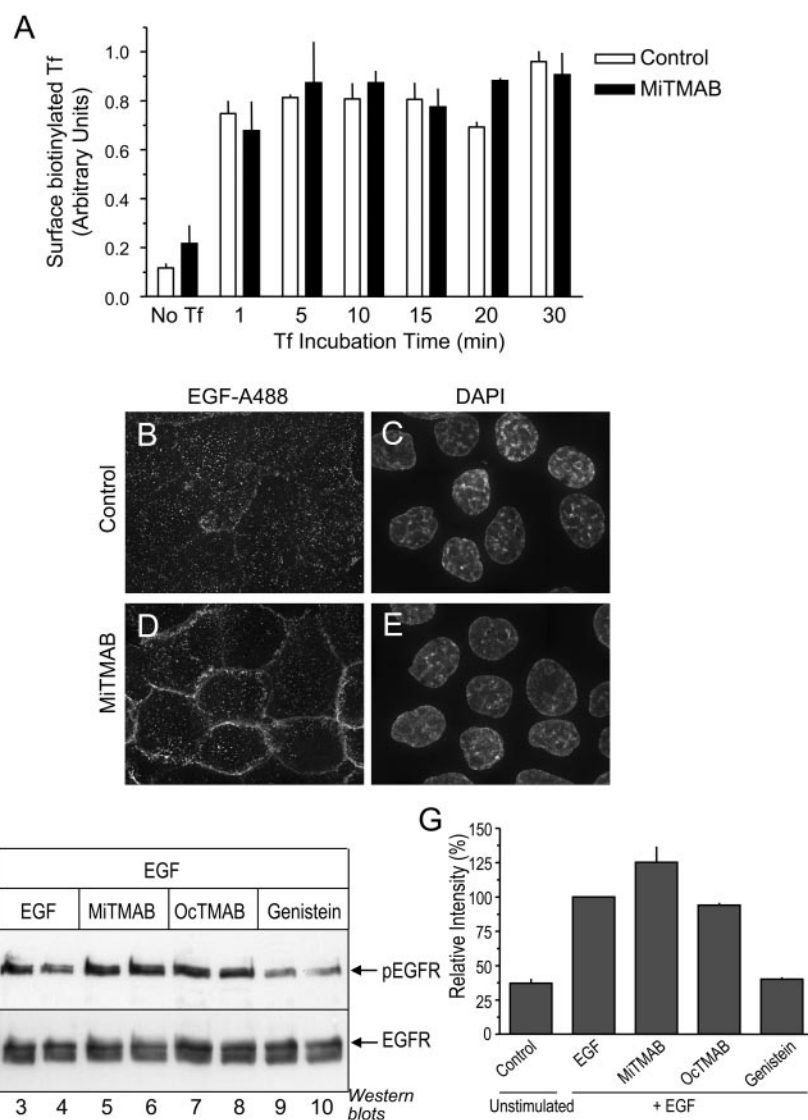


**Fig. 4.** MiTMAB does not block Tf and EGF binding and EGFR activation. **A**, Tf binding assay. COS-7 cells were either preincubated with DMSO (control) or MiTMAB (30  $\mu$ M for 10 min) at 37°C, then incubated for different times with biotinylated-Tf (10  $\mu$ g/ml) on ice for Tf cell surface binding. Cell lysates were analyzed by Western blot and probed with avidin-HRP to detect the amount of biotinylated-Tf in cell lysates. Blots were quantitated using densitometry, and the intensity (arbitrary units) of the biotinylated-Tf was normalized against an endogenous biotinylated protein on the blots. The average of the range of values is plotted. Error bars indicate the range of values ( $n = 2$ ). **B** to **E**, surface EGF binding assay. A431 cells were preincubated with DMSO (control) (**B** and **C**) or 30  $\mu$ M MiTMAB (**D** and **E**) for 10 min at 37°C, then placed on ice and incubated with 600 ng/ml EGF-A488 for 30 min, fixed in 4% PFA at room temperature (22°C), and counterstained with DAPI. Images are maximum projection images generated from three-dimensional deconvolution of Z-stack images and are representative of two independent experiments. **F**, Western blots of pEGFR and total endogenous EGFR levels in A431 cell lysates preincubated without (control) or with MiTMAB, OcTMAB, or genistein (negative control; each drug at 30  $\mu$ M) for 10 min at 37°C, and then stimulated with 100 ng/ml EGF. **G**, densitometry analysis of the blots. The intensity of the EGFR phosphorylation signals were normalized to their respective total EGFR signals, then expressed as a relative intensity (percentage) of the EGF-stimulated control sample. Error bars indicate the range of values ( $n = 2$ ).

microscopy. Expression of GFP-dyn I-PH domain in control cells revealed a predominantly cytosolic distribution as expected, but a significant pool was specifically associated with the plasma membrane in all cells (Fig. 5, A and B). Higher magnification of the boxed regions illustrates the membrane association (Fig. 5, A' and B'). When cells were treated with MiTMAB at 30  $\mu$ M for 30 min, the staining of the plasma membrane was abolished (Fig. 5, C and D, boxed region, and zoomed regions in Fig. 5, C' and D'). The inactive analog myristic acid at 30  $\mu$ M had no effect (Fig. 5, E and F, boxed region, and zoomed regions in Fig. 5, E' and F'). Therefore, MiTMAB prevented GFP-dyn I-PH domain localization to the plasma membrane of HeLa cells, suggesting that the arrest of RME was due to blocking dynamin recruitment to the membrane. To confirm that transfection alone of the GFP-dyn I-PH domain construct did not block RME, endocytosis of Tf-A594 and EGF-TxR was monitored simultaneously in these experiments (Supplemental Figure S1). RME was unaffected by transfection alone, but it was almost abolished in the cells treated with MiTMAB. In contrast, cells treated with myristic acid showed normal Tf internalization (data not shown). Next, we examined the effect of MiTMAB on an unrelated PH domain protein with high affinity for membrane phospholipids, PLC $\delta$ 1-PH domain (Garcia et al., 1995). MiTMAB also blocked its localization to the plasma membrane in HeLa cells, and myristic acid was without effect (Supplemental Figure S2). This suggests that MiTMAB inhibits the PH domain-phospholipid interactions of proteins in addition to dynamin.

**MiTMAB Blocked KCl-Induced Exocytosis in Rat Adrenal Chromaffin Cells.** To determine whether MiTMAB inhibits SVE, we used two models for neuronal exocytosis and endocytosis. First, we investigated whether MiTMAB inhibited endocytosis in adrenal chromaffin cells, a neuroen-

docrine cell that releases catecholamines on depolarization, which can be monitored using carbon fiber amperometry because of the charged nature of catecholamines. Because exocytosis and endocytosis are coupled in such excitable cells, it is first necessary to determine the effects on exocytosis of any potential inhibitor, before determining its effect on endocytosis. A block in the former will nonspecifically inhibit the latter, masking any specific endocytic effect. The chromaffin cells robustly secreted catecholamines in response to a first 70 mM KCl (S1) stimulus (Fig. 6A). The same magnitude of exocytosis was reproducibly observed after a second (S2) (Fig. 6A) or third (S3) stimulation (data not shown). However, when 30  $\mu$ M MiTMAB was applied for 10 min between stimuli, surprisingly, exocytosis was abolished at S2 (Fig. 6B). Quantitative analysis of the number of events per minute and total charge due to catecholamine release revealed the strong exocytosis inhibition (Fig. 6, C and D). The compound did not induce exocytosis on its own or depolarize the cells, suggesting that the membrane potential was intact. Because KCl-induced exocytosis is dependent on  $\text{Ca}^{2+}$  entry, we explored this as a potential mechanism for the effect. Chromaffin cells were loaded with the  $\text{Ca}^{2+}$ -sensitive fluorescent dye Fluo-3. Fluorescence increases, indicative of increased intracellular  $\text{Ca}^{2+}$  concentrations, were observed upon stimulation with 70 mM KCl for 1 min (Fig. 6E). However, high-KCl-induced  $\text{Ca}^{2+}$  entry was abolished after 10-min incubation with MiTMAB. This was not due to an immediate extracellular ion channel pore block by MiTMAB, because a significant amount of  $\text{Ca}^{2+}$  entry still occurred ( $p < 0.01$ ), albeit at 20% of the original value, in cells after just 1-min incubation with MiTMAB ( $n = 10$ ; Fig. 6F). The results reveal that MiTMAB blocks exocytosis in chromaffin cells by reducing  $\text{Ca}^{2+}$  entry via an intracellular site of action, presumably  $\text{Ca}^{2+}$  channels. The data also indicate that the effect

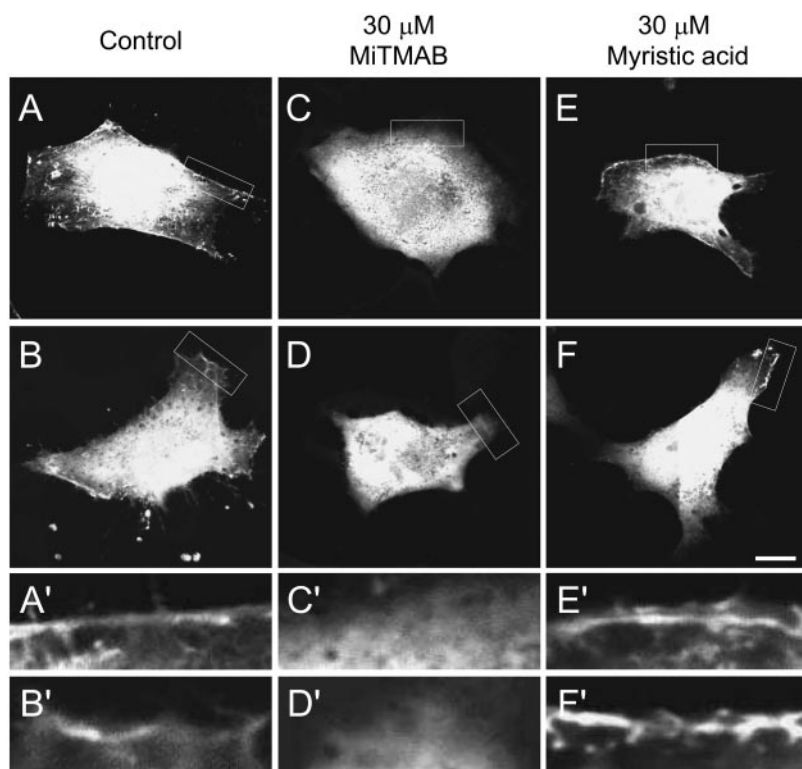


**Fig. 5.** MiTMAB prevents PH domain localization on plasma membranes. HeLa cells were transfected with GFP-dyn I-PH domain (A and B), then incubated with 30  $\mu$ M MiTMAB (C and D) or 30  $\mu$ M myristic acid (E and F) at 37°C for 30 min. The distribution of GFP-dyn I-PH domain was detected by confocal fluorescence microscopy. Top and middle rows, representative images of single cells from two independent experiments. Although most of the expressed protein was cytosolic, a significant membrane distribution is evident in all control cells. Boxes indicate regions of the plasma membrane that are shown at higher magnification in the bottom panels. The same results were obtained in three independent experiments. Scale bar, 10  $\mu$ m (A–F).

of MiTMAB on endocytosis cannot be assessed in these particular cells.

**MiTMAB Blocked SVE but Not Exocytosis in Synaptosomes.** The  $\text{Ca}^{2+}$  channels and other voltage-regulated ion channels in distinct cell types are different. Therefore, we examined the effect of MiTMAB on SVE in a population of rat brain nerve terminals (synaptosomes) using styryl dye approaches. We first examined endogenous glutamate release, and we found that preincubation with 30  $\mu\text{M}$  MiTMAB for 10 min had no effect on KCl-evoked  $\text{Ca}^{2+}$ -dependent glutamate release and thus SV exocytosis (Fig. 7A). SVE was monitored using an established SV turnover assay that uses the activity-dependent dye FM2-10 (Cousin and Robinson, 2000). MiTMAB significantly reduced KCl-evoked uptake of FM2-10 compared with control (Fig. 7B). Because FM2-10 uptake reflects not only on SVE but also the prior round of exocytosis, we appraised the specific effect of MiTMAB on SVE by calculating retrieval efficiency, which is a ratio of the

amount of SVE divided by amount of exocytosis (Cousin and Robinson, 2000), where a value less than 1 indicates a selective SVE inhibition. MiTMAB significantly reduced retrieval efficiency to  $0.76 \pm 0.08$  (Fig. 7C), indicative of specific block in SVE. Therefore, MiTMAB selectively blocks SVE but not exocytosis in synaptosomes.

To confirm the block in SVE in synaptosomes by an independent approach, we used an electron microscopy-based method to reveal inhibition of SVE in synaptosomes (Tan et al., 2003). Synaptosomes at rest or depolarized with KCl for 2 min exhibited normal morphology by electron microscopy (Fig. 7, D and E). Normal nerve terminals were characterized by 1) a smooth, sealed plasma membrane; 2) being mostly filled with small SVs; 3) almost always containing one or more normal mitochondrial profiles; and 4) occasionally containing a synapse and associated postsynaptic density (if sectioned at the appropriate angle). We found that pretreatment with 30  $\mu\text{M}$  MiTMAB had no effect on nerve terminal

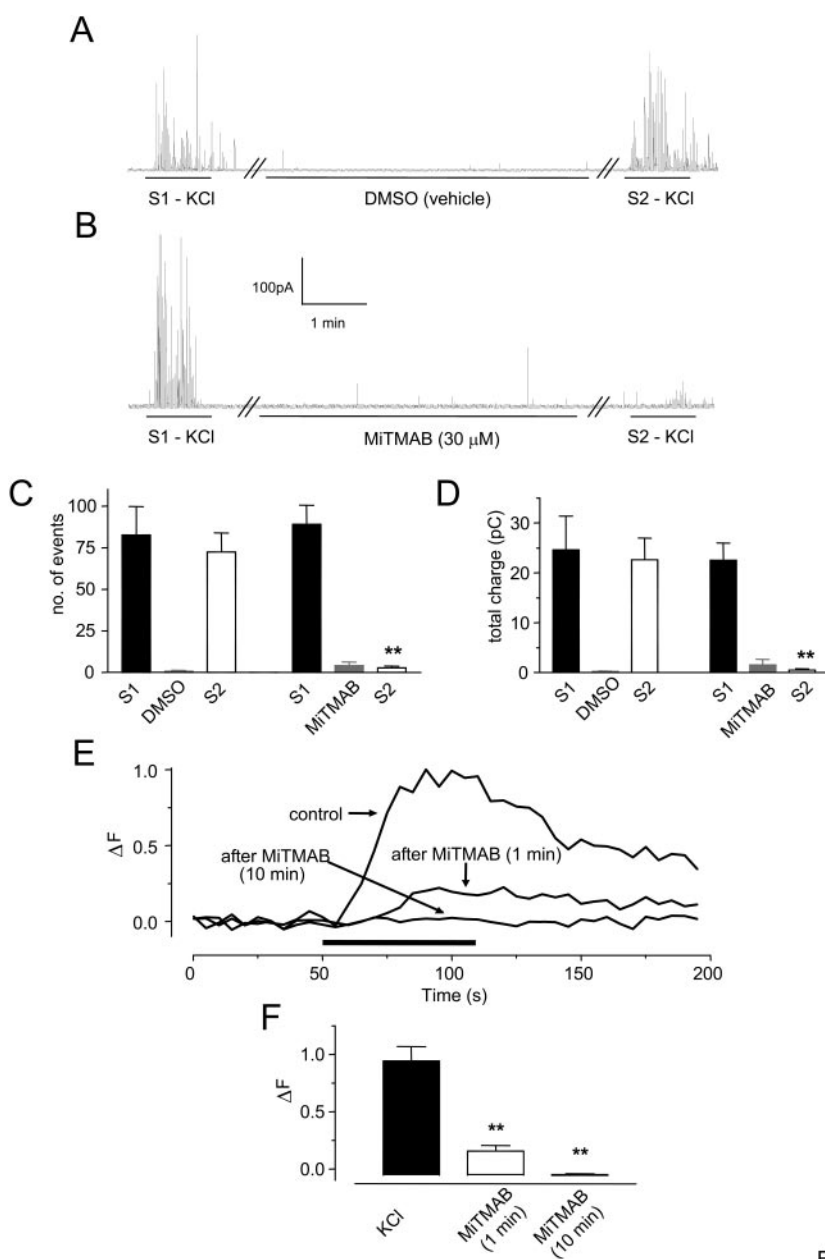


**Fig. 6.** MiTMAB inhibits exocytosis and  $\text{Ca}^{2+}$  entry in chromaffin cells. A and B, carbon fiber amperometry was used to measure catecholamine release (shown as spikes) from single rat adrenal chromaffin cells induced by two pulses of high-KCl (70 mM) bath solution for 1 min (S1 and S2). Double sloped lines at the bottom of the traces indicate a break in recording. After the first stimulation, cells were washed for 5 min, and then they were exposed for 10 min to a solution containing either 30  $\mu\text{M}$  MiTMAB in 0.3% DMSO (B) or an equivalent volume of DMSO in bath solution (A). The results are summarized for both the number of secretory events (C) and the total amount of charge released (D) in 1 min ( $n = 9$  for both control and MiTMAB-treated cells). The results for DMSO or MiTMAB alone are over a 10-min period and represent all recorded cells. E, fluorescence of cells loaded with Fluo-3 increased significantly upon exposure to high-KCl (70 mM) solution (the period of stimulation is indicated by a solid bar). The effect of preincubation with MiTMAB for 1 or 10 min is shown. F, quantitative analysis of the  $\text{Ca}^{2+}$  results such as in E. The absolute change in fluorescence due to  $\text{Ca}^{2+}$  influx ( $\Delta F$ ) is shown as mean  $\pm$  S.D. ( $n = 14$ , 10, and 14 cells for each column left to right). \*\*,  $p < 0.001$ , significantly less than S1 value.



morphology in resting (unstimulated) synaptosomes (Fig. 7F). However, when the synaptosomes were depolarized with 30 mM KCl for 2 min after MiTMAB pretreatment, there was a massive depletion of SVs, consistent with a specific SVE block (Fig. 7, G–I). This confirms that MiTMAB inhibits dynamin I-dependent SVE in synaptosomes.

## Discussion

The large GTPases dynamin I and II are essential for many forms of membrane internalization in eukaryotic cells (Hinsch, 2000). Therefore, small-molecule inhibitors with different mechanisms of action on these key enzymes should prove to be important tools for greater understanding of their function during normal and abnormal processes. We previously reported on a series of long-chain ammonium salts, such as MiTMAB and OcTMAB, as the first small-molecule dynamin inhibitors (Hill et al., 2004). We have now extended this observation to demonstrate that MiTMAB is a surface-active compound that targets the dynamin-phospholipid association and that it is a potent inhibitor of at least two forms

of endocytosis in cells: RME and SVE. The compounds act rapidly to inhibit endocytosis in cells, and their effects are rapidly reversed after short washout. The  $K_i$  for MiTMAB was in the high nanomolar range, indicating that it has relatively high intrinsic affinity for dynamin. The activity of these compounds partly correlated with alkyl chain length, and it was dependent on an amine or ammonium salt head group rather than an acid. The results provide a range of compounds with distinct potencies allowing a correlation between their *in vitro* and *in vivo* actions.

The interaction of dynamin with phospholipids is mediated by its PH domain. PH domains of proteins are known to bind acidic phospholipids, especially phosphatidylserine and specific phosphoinositides (Zheng et al., 1996; Lemmon, 2003), and the PH domain of dynamin has highest affinity for  $\text{PtdIns}(4,5)\text{P}_2$  (Salim et al., 1996; Barylko et al., 1998). Lipid binding promotes dynamin oligomerization, which stimulates its GTPase activity (Klein et al., 1998). Using three independent approaches, we attribute the mechanism of action of MiTMAB to inhibition of the dynamin-phospholipid

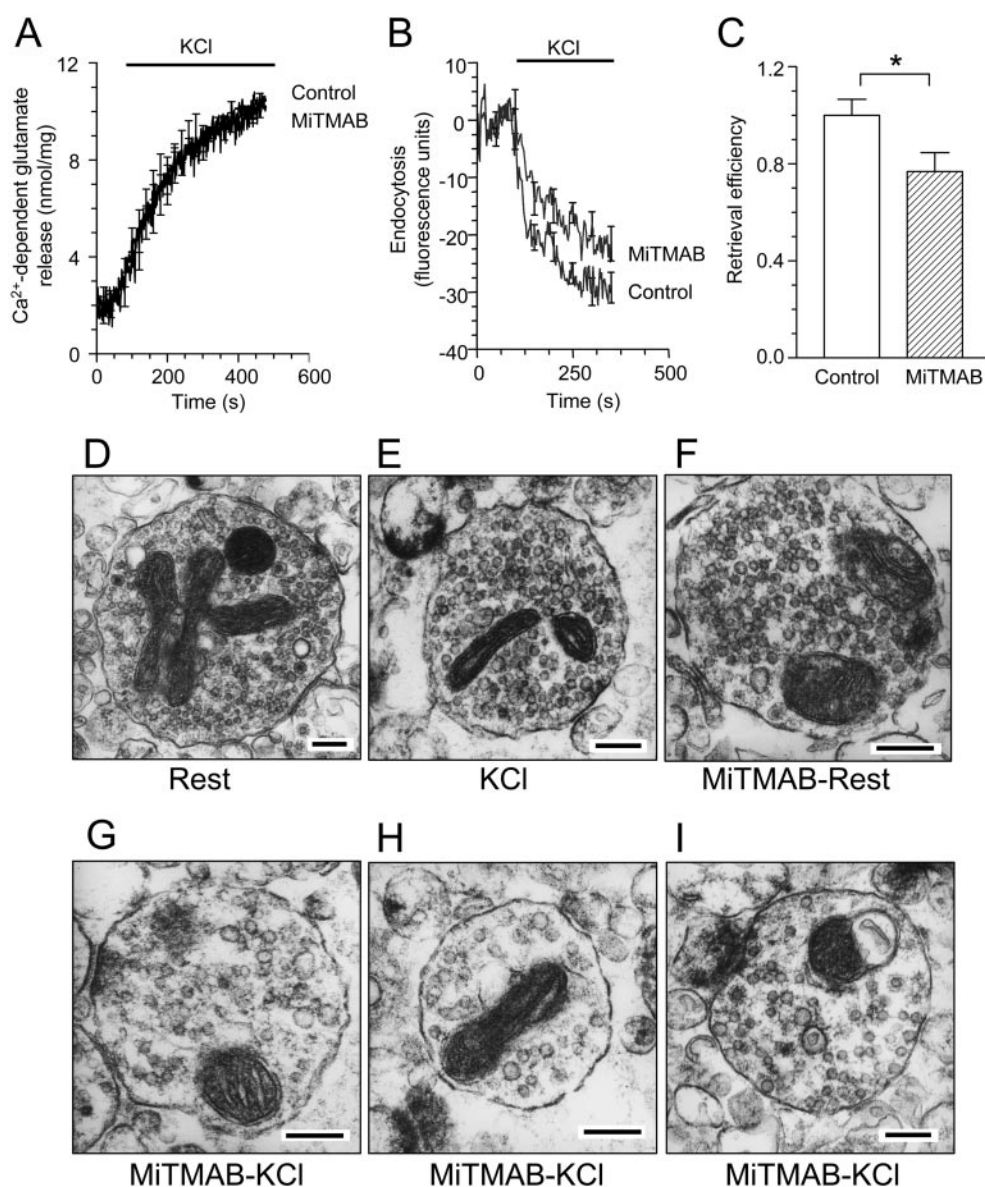


**Fig. 7.** MiTMAB inhibits SVE but not exocytosis in synaptosomes. **A**, synaptosomes were preincubated with 30  $\mu\text{M}$  MiTMAB for 10 min before stimulation with 30 mM KCl. The effect on SV exocytosis (calcium-dependent glutamate release) is displayed in the absence (control) or presence of MiTMAB. **B**, synaptosomes were incubated with or without 30  $\mu\text{M}$  MiTMAB for 10 min, and then they were loaded with FM2-10 using a 2-min KCl stimulus, and the extent of loading (endocytosis) was estimated with a subsequent unloading stimulus to release the accumulated dye (Cousin and Robinson, 2000). Endocytosis (calcium-dependent uptake and release of FM2-10) in the absence or presence of MiTMAB is shown as the decrease in fluorescence. The bar in **A** and **B** denotes the presence of KCl. **(C)** Retrieval efficiency (endocytosis divided by exocytosis) was significantly inhibited (\*,  $p < 0.05$ ;  $n = 5 \pm \text{S.E.M.}$ ), indicating a specific block in SVE. **D** to **I**, effect of MiTMAB on synaptosome morphology. Synaptosomes were treated with vehicle alone (**D** and **E**) or 30  $\mu\text{M}$  MiTMAB for 5 min (**F**–**I**), and then they were incubated in control buffer (i.e., at “rest”) (**D** and **F**), or they were depolarized with 30 mM KCl for 2 min (**E** and **G**–**I**). Synaptosomes were pelleted and fixed for electron microscopy. Images are representative of two independent experiments. Scale bars, 200 nm.

interaction. First, MiTMAB was without effect on the elevated nonstimulated GTPase activity of dynamin I- $\Delta$ PH. Second, MiTMAB blocked dynamin binding to phospholipid *in vitro*. Finally, enzyme kinetics showed that MiTMAB is a competitive inhibitor with PS and noncompetitive with GTP. The three observations establish that MiTMAB directly interferes with PH domain binding to the phospholipid, as may have been expected for surface active cationic amphiphilic compounds. These *in vitro* observations were correlated in cells by expression of the dynamin I-PH domain. The binding of this domain to the cell membrane was abolished by MiTMAB but not by the inactive myristic acid.

In non-neuronal cells, we found that MiTMAB inhibits Tf and EGF internalization in a variety of cell lines, suggesting a wide utility for such inhibitors as broad-spectrum endocytosis inhibitors. RME is known to be dependent on the interaction of the PH domain of dynamin II with membrane phospholipids (Lee et al., 1999; Vallis et al., 1999), suggesting this association is the target for MiTMAB. Two further lines of evidence suggested the RME inhibition in cells occurred via inhibition of the dynamin-phospholipid interaction. First, the rank order of potency of five of the six analogs on RME precisely correlated with the order of their IC<sub>50</sub> values for dynamin inhibition. Second, MiTMAB blocked membrane binding by the dynamin I PH domain in HeLa cells, driving it to the cytosol where it cannot support endocytosis. Thus, we propose that the MiTMAB series of compounds arrest RME by interfering with the dynamin-phospholipid interaction. In contrast to the other compounds, 2-(dimethylamino) ethyl myristate was effective *in vitro*, but it did not have any *in vivo* activity. It was designed as a prodrug for intracellular delivery of myristic acid. The compound is expected to be fully membrane-permeable, but presumably it was rapidly cleaved to myristic acid (which is inactive) and dimethyl amino ethanol by endogenous intracellular esterases, in a manner similar to other prodrug esters such as Fura2-AM or BAPTA-AM. Therefore, this compound will be useful as a negative control in future cellular studies.

Another well characterized endocytic route is SVE, in which the role of dynamin I has been well established (Tan et al., 2003; Anggono et al., 2006). In these systems, exocytosis and endocytosis are highly regulated and coupled; thus, blocking one route interferes with the other (Anggono et al., 2006). We therefore examined exocytosis in two systems, chromaffin cells and rat brain nerve terminals (synaptosomes). We were surprised to find that MiTMAB blocked exocytosis in chromaffin cells by preventing Ca<sup>2+</sup> influx; hence, its effect on endocytosis could not be further evaluated. Despite this, the results indicate that the compound does not cause membrane damage to the cells, because basal capacitance and low intracellular Ca<sup>2+</sup> concentrations were maintained in the presence of the drug. These are both independent indices of an intact plasma membrane. However, exocytosis of glutamate from synaptosomes was unaffected. This further indicates that the drug does not disrupt membrane structure, because normal membrane potential was maintained in the presence of the drug. MiTMAB inhibited synaptosomal SVE by two independent criteria: styryl dye uptake, and it produced morphological depletion of synaptic vesicles. Overall, our data indicate that MiTMAB inhibits two mechanistically distinct forms of endocytosis via inhibition of dynamin I or dynamin II GTPase activity. The further

potential for MiTMAB to block endocytosis in animals was recently demonstrated (Hilliard et al., 2006). Perfusion of exteriorized kidney with MiTMAB increased excretion of intact albumin. This suggests that MiTMAB blocks albumin endocytosis in an organ still attached to a living animal. This illustrates the potential application of an RME inhibitor such as MiTMAB to studies investigating a previously unknown involvement of RME in cellular pathways.

The long-chain amines and ammonium salts reported here are amphiphilic compounds with either a nonionic [2-(dimethylamino) ethyl myristate, tetradecylamine] or a cationic polar (DoTMAB, MiTMAB, and OcTMAB) head group and a hydrophobic tail. Many drugs of clinical importance have nonionic or cationic amphiphilic properties (Fischer et al., 1998; Schreier et al., 2000; Ahyauch et al., 2002). Studies into the molecular mechanisms of pharmacological effects exerted by drugs of such structure commonly reveal they have surface-active properties, such as self-aggregation and the ability to interact with membranes. These properties are characterized by physicochemical parameters, such as the cmc, aggregation number, and particle size (Schreier et al., 2000). Self-aggregation in aqueous medium and surface absorption kinetics on an artificial silica-aqueous interface have been previously studied for the MiTMAB series (Atkin et al., 2003). The cmc values for DoTMAB, MiTMAB, and OcTMAB are 6.3, 1, and 0.2 mM, respectively (in aqueous medium containing 10 mM potassium bromide), indicating that cmc decreases as the chain length of the hydrophobic tail increases (Atkin et al., 2003). At high concentrations above its cmc, MiTMAB forms mixed micelles and aggregates. The correlation between the cmc of a compound and the formation of micelle aggregates is significant to the understanding of potential membrane lipid effects of the drug, because disruption of lipid bilayer membranes may be modulated by micelle-like aggregates (Schreier et al., 2000). At high concentrations above the cmc, other cationic amphiphilic compounds, such as chlorpromazine and imipramine, exhibit membrane-solubilizing effects that are distinct from their medicinal or biological effects by 1 to 3 orders of magnitude (Ahyauch et al., 2002). Many lines of evidence suggest that the *in vitro* and *in vivo* inhibitory effects of MiTMAB are not a result of the compound acting like a classic detergent, solubilizing phospholipids, and disrupting cell membranes. First, the IC<sub>50</sub> for dynamin inhibition is >300-fold below the cmc. Second, the two sets of nonionic and cationic head groups provide these compounds with completely different surface-active and binding properties; yet, both sets are effective dynamin and endocytosis inhibitors within a narrow potency range. Third, in the synaptosomal SVE assay, Ca<sup>2+</sup>-dependent glutamate release was not blocked by MiTMAB, indicating a preserved membrane potential, produced by Na<sup>+</sup>, K<sup>+</sup>, and Ca<sup>2+</sup> gradients. Electron micrographs show that the membranes of the synaptosomes remained intact and undamaged, indicating MiTMAB did not exhibit any membrane-solubilizing properties at such low concentrations. Fourth, MiTMAB induced no cell or membrane damage to COS-7, HeLa, A431, or the excitable chromaffin cells, again suggesting the cells were otherwise viable. Finally, the effects of the drugs on endocytosis were rapidly and fully reversible. Because RME is capable of starting again, this indicates the presence of relatively healthy cells.

There are potential nonspecific actions of all drugs that



must be considered in their application to living tissues. MiTMAB blocked  $\text{Ca}^{2+}$  influx into chromaffin cells but not synaptosomes. The target was intramembrane and intracellular. The block could be a voltage-gated ion channel, such as the  $\text{Ca}^{2+}$  channel, because KCl depolarizes membranes and activates such channels directly. Most drugs have such secondary effects, and they need to be taken into consideration in experimental design. First, for example, the potent Cdk5 inhibitor roscovitine (Tan et al., 2003) also inhibits P/Q-type  $\text{Ca}^{2+}$  channels (Yan et al., 2002); yet, this does not diminish its broad utility in cell biology apart from its use in certain cultured neurons (Tan et al., 2003). Second, a drug that targets the dynamin-phospholipid interaction will probably have effects on other intracellular phospholipid binding enzymes such as we found for the PH domain of PLC $\delta$ 1. Third, although MiTMAB did not block EGF receptor signal transduction or extracellular ligand binding to cell surface receptors, it altered the cell surface clustering of EGF receptors. Therefore, the surface-active properties of MiTMAB can produce nonspecific effects on plasma membranes with different phospholipid compositions, possibly causing membrane reorganization effects in some cells. For example, antidepressants, such as clomipramine and imipramine, have micellar properties, and membrane interaction effects that regulate the side effects of the drug (Attwood et al., 1995; Ahyauch et al., 2002).

In summary, we have identified and characterized a series of long-chain amine salts as inhibitors of dynamin GTPase activity, which act by preventing dynamin association with phospholipid membranes. Because treatment of neuronal and non-neuronal cells with these small-molecule compounds rapidly and reversibly blocks multiple forms of endocytosis (RME and SVE), they will be useful tools to probe the function of dynamin I and II, not only in endocytosis, but for its numerous intracellular functions, such as phagocytosis, post-Golgi transport, podosomes, cell migration, and invasion. The MiTMAB series will also be useful for understanding the potential roles of dynamin in disease states such as cancer, inflammation, and neuropsychiatric and neurodegenerative disorders. Small molecule endocytosis inhibitors such as the MiTMAB series provide significant new cell biological tools for further molecular dissection of membrane trafficking and endocytosis pathways in eukaryotic cells.

## Acknowledgments

We thank Peter Rowe for encouragement and helpful comments on the manuscript and our colleagues who provided enzymes and plasmid DNA. We also thank Ross Boadle and Levina Deer for valuable technical assistance with electron microscopy.

## References

- Achiriloae M, Barylko B, and Albanesi JP (1999) Essential role of the dynamin pleckstrin homology domain in receptor-mediated endocytosis. *Mol Cell Biol* **19**: 1410–1415.
- Ahyauch H, Requero MA, Alonso A, Bennouna M, and Goni FM (2002) Surfactant effects of chlorpromazine and imipramine on lipid bilayers containing sphingomyelin and cholesterol. *J Colloid Interface Sci* **256**:284–289.
- Anggono V, Smillie KJ, Graham ME, Valova VA, Cousin MA, and Robinson PJ (2006) Syndapin I is the phosphorylation-regulated dynamin i partner in synaptic vesicle endocytosis. *Nat Neurosci* **9**:752–760.
- Artalejo CR, Lemmon MA, Schlessinger J, and Palfrey HC (1997) Specific role for the PH domain of dynamin-1 in the regulation of rapid endocytosis in adrenal chromaffin cells. *EMBO J* **16**:1565–1574.
- Atkin R, Craig VS, Wanless EJ, and Biggs S (2003) The influence of chain length and electrolyte on the adsorption kinetics of cationic surfactants at the silica-aqueous solution interface. *J Colloid Interface Sci* **266**:236–244.
- Attwood D, Mosquera V, Garcia M, Suarez MJ, and Sarmiento F (1995) A comparison of the micellar properties of structurally related antidepressant drugs. *J Colloid Interface Sci* **175**:201–262.
- Atwood WJ (2001) A combination of low-dose chlorpromazine and neutralizing antibodies inhibits the spread of JC virus (JCV) in a tissue culture model: implications for prophylactic and therapeutic treatment of progressive multifocal leukoencephalopathy. *J Neurovirol* **7**:307–310.
- Barylko B, Binns DD, Lin KM, Atkinson ML, Jameson DM, Yin HL, and Albanesi JP (1998) Synergistic activation of dynamin GTPase by Grb2 and phosphoinositides. *J Biol Chem* **273**:3791–3797.
- Chow RH, von Ruden L, and Neher E (1992) Delay in vesicle fusion revealed by electrochemical monitoring of single secretory events in adrenal chromaffin cells. *Nature* **356**:60–63.
- Cousin MA and Robinson PJ (1998)  $\text{Ba}^{2+}$  does not support synaptic vesicle retrieval in rat isolated presynaptic nerve terminals. *Neurosci Lett* **253**:1–4.
- Cousin MA and Robinson PJ (2000)  $\text{Ca}^{2+}$  inhibition of dynamin arrests synaptic vesicle recycling at the active zone. *J Neurosci* **20**:949–957.
- Cousin MA and Robinson PJ (2001) The dephosphins: dephosphorylation by calcineurin triggers synaptic vesicle endocytosis. *Trends Neurosci* **24**:659–665.
- Danke H, Binns DD, Ueda H, Schmid SL, and Baba T (2001) Dynamin GTPase domain mutants block endocytic vesicle formation at morphologically distinct stages. *Mol Biol Cell* **12**:2578–2589.
- Davies PJ, Cornwell MM, Johnson JD, Reggianni A, Myers M, and Murtaugh MP (1984) Studies on the effects of dansylcadaverine and related compounds on receptor-mediated endocytosis in cultured cells. *Diabetes Care* **7** (Suppl 1):35–41.
- Dunkley PR, Jarvie PE, Heath JW, Kidd GJ, and Rostas JA (1986) A rapid method for isolation of synaptosomes on Percoll gradients. *Brain Res* **372**:115–129.
- Ferguson SM, Brasnjic G, Hyashi M, Wolfel M, Collesi C, Giovedi S, Raimondi A, Gong LW, Arell P, Paradise S, et al. (2007) A selective activity-dependent requirement for dynamin 1 in synaptic vesicle endocytosis. *Science* **316**:570–574.
- Fischer H, Gottschlich R, and Seelig A (1998) Blood-brain barrier permeation: molecular parameters governing passive diffusion. *J Membr Biol* **165**:201–211.
- Gáborik Z and Hunyady L (2004) Intracellular trafficking of hormone receptors. *Trends Endocrinol Metab* **15**:286–293.
- Garcia P, Gupta R, Shah S, Morris AJ, Rudge SA, Scarlata S, Petrova V, McLaughlin S, and Rebecchi MJ (1995) The pleckstrin homology domain of phospholipase C- $\delta$ 1 binds with high affinity to phosphatidylinositol 4,5-bisphosphate in bilayer membranes. *Biochemistry* **34**:16228–16234.
- Geladopoulos TP, Sotiropoulos TG, and Evangelopoulos AE (1991) A malachite green colorimetric assay for protein phosphatase activity. *Anal Biochem* **192**:112–116.
- Gray JA, Sheffler DJ, Bhatnagar A, Woods JA, Hufeisen SJ, Benovic JL, and Roth BL (2001) Cell-type specific effects of endocytosis inhibitors on 5-hydroxytryptamine $_2$  receptor desensitization and resensitization reveal an arrestin-, GRK2-, and GRK5-independent mode of regulation in human embryonic kidney 293 Cells. *Mol Pharmacol* **60**:1020–1030.
- Hill TA, Odell LR, Edwards JK, Graham ME, McGeachie AB, Rusak J, Quan A, Abagyan R, Scott JL, Robinson PJ, et al. (2005) Small molecule inhibitors of dynamin i GTPase activity: development of dimeric tyrosinophostins. *J Med Chem* **48**:7781–7788.
- Hill TA, Odell LR, Quan A, Abagyan R, Ferguson G, Robinson PJ, and McCluskey A (2004) Long chain amines and long chain ammonium salts as novel inhibitors of dynamin GTPase activity. *Bioorg Med Chem Lett* **14**:3275–3278.
- Hilliard LM, Osicka TM, Robinson PJ, Nikolic-Paterson DJ, and Comper WD (2006) Characterisation of the urinary degradation pathway in the isolated perfused rat kidney. *J Lab Clin Med* **147**:36–44.
- Hinshaw JE (2000) Dynamin and its role in membrane fission. *Annu Rev Cell Dev Biol* **16**:483–519.
- Hohenwallner W and Wimmer E (1973) The malachite green micromethod for the determination of inorganic phosphate. *Clin Chim Acta* **45**:169–175.
- Jockusch WJ, Praefcke GJ, McMahon HT, and Lagnado L (2005) Clathrin-dependent and clathrin-independent retrieval of synaptic vesicles in retinal bipolar cells. *Neuron* **46**:869–878.
- Kaksonen M, Toret CP, and Drubin DG (2006) Harnessing actin dynamics for clathrin-mediated endocytosis. *Nat Rev Mol Cell Biol* **7**:404–414.
- Keating DJ, Rychkov GY, and Roberts ML (2001) Oxygen sensitivity in the sheep adrenal medulla: role of SK channels. *Am J Physiol Cell Physiol* **281**:C1434–C1441.
- Klein DE, Lee A, Frank DW, Marks MS, and Lemmon MA (1998) The pleckstrin homology domains of dynamin isoforms require oligomerization for high affinity phosphoinositide binding. *J Biol Chem* **273**:27725–27733.
- Koenig JH and Ikeda K (1989) Disappearance and reformation of synaptic vesicle membrane upon transmitter release observed under reversible blockage of membrane retrieval. *J Neurosci* **9**:3844–3860.
- Larkin JM, Brown MS, Goldstein JL, and Anderson RG (1983) Depletion of intracellular potassium arrests coated pit formation and receptor-mediated endocytosis in fibroblasts. *Cell* **33**:273–285.
- Le Roy C and Wrana JL (2005) Clathrin- and non-clathrin-mediated endocytic regulation of cell signalling. *Nat Rev Mol Cell Biol* **6**:112–126.
- Lee A, Frank DW, Marks MS, and Lemmon MA (1999) Dominant-negative inhibition of receptor-mediated endocytosis by a dynamin-1 mutant with a defective pleckstrin homology domain. *Curr Biol* **9**:261–264.
- Lemmon MA (2003) Phosphoinositide recognition domains. *Traffic* **4**:201–213.
- Lin HC, Barylko B, Achiriloae M, and Albanesi JP (1997) Phosphatidylinositol (4,5)-bisphosphate-dependent activation of dynamin I and II lacking the proline/arginine-rich domains. *J Biol Chem* **272**:25999–26004.
- Lindgren CA, Emery DG, and Haydon PG (1997) Intracellular acidification reversibly reduces endocytosis at the neuromuscular junction. *J Neurosci* **17**:3074–3084.
- Liu JP and Robinson PJ (1995) Dynamin and endocytosis. *Endocr Rev* **16**:590–607.
- Marks B and McMahon HT (1998) Calcium triggers calcineurin-dependent synaptic vesicle recycling in mammalian nerve terminals. *Curr Biol* **8**:740–749.
- Marks B, Stowell MH, Vallis Y, Mills IG, Gibson A, Hopkins CR, and McMahon HT



- (2001) GTPase activity of dynamain and resulting conformation change are essential for endocytosis. *Nature* **410**:231–235.
- McNiven MA (1998) Dynamain: a molecular motor with pinchose action. *Cell* **94**:151–154.
- Nicholls DG and Sihra TS (1986) Synaptosomes possess an exocytotic pool of glutamate. *Nature* **321**:772–773.
- Quan A and Robinson PJ (2005) Rapid purification of native dynamain I and colorimetric GTPase assay. *Methods Enzymol* **404**:556–569.
- Robinson PJ, Sontag J-M, Liu JP, Fykse EM, Slaughter C, McMahon HT, and Südhof TC (1993) Dynamain GTPase regulated by protein kinase C phosphorylation in nerve terminals. *Nature* **365**:163–166.
- Roux A, Uyhazi K, Frost A, and De Camilli P (2006) GTP-dependent twisting of dynamain implicates constriction and tension in membrane fission. *Nature* **441**:528–531.
- Salim K, Bottomley MJ, Querfurth E, Zvelebil MJ, Gout I, Scaife R, Margolis RL, Gigg R, Smith CI E, Driscoll PC, et al. (1996) Distinct specificity in the recognition of phosphoinositides by the pleckstrin homology domains of dynamain and Bruton's tyrosine kinase. *EMBO J* **15**:6241–6250.
- Scaife R, Venien-Bryan C, and Margolis RL (1998) Dual function C-terminal domain of dynamain-1: modulation of self-assembly by interaction of the assembly site with SH3 domains. *Biochemistry* **37**:17673–17679.
- Schreier S, Malheiros SV and de Paula E (2000) Surface active drugs: self-association and interaction with membranes and surfactants. Physicochemical and biological aspects. *Biochim Biophys Acta* **1508**:210–234.
- Scurlock JE and Curtis BM (1981) Tetraethylammonium derivatives: ultralong-acting local anesthetics? *Anesthesiology* **54**:265–269.
- Sheff D, Pelletier L, O'Connell CB, Warren G, and Mellman I (2002) Transferrin receptor recycling in the absence of perinuclear recycling endosomes. *J Cell Biol* **156**:797–804.
- Stowell MH, Marks B, Wigge P, and McMahon HT (1999) Nucleotide-dependent conformational changes in dynamain: evidence for a mechanochemical molecular spring. *Nat Cell Biol* **1**:27–32.
- Tan TC, Valova VA, Malladi CS, Graham ME, Berven LA, Jupp OJ, Hansra G, McClure SJ, Sarcevic B, Boadle RA, et al. (2003) Cdk5 is essential for synaptic vesicle endocytosis. *Nat Cell Biol* **5**:701–710.
- Trowbridge IS, Collawn JF, and Hopkins CR (1993) Signal-dependent membrane protein trafficking in the endocytic pathway. *Annu Rev Cell Biol* **9**:129–161.
- Vallis Y, Wigge P, Marks B, Evans PR, and McMahon HT (1999) Importance of the pleckstrin homology domain of dynamain in clathrin-mediated endocytosis. *Curr Biol* **9**:257–260.
- van der Bliek AM, Redelmeier TE, Damke H, Tisdale EJ, Meyerowitz EM, and Schmid SL (1993) Mutations in human dynamain block an intermediate stage in coated vesicle formation. *J Cell Biol* **122**:553–563.
- Van Veldhoven PP and Mannaerts GP (1987) Inorganic and organic phosphate measurements in the nanomolar range. *Anal Biochem* **161**:45–48.
- Wang L-H, Rothberg KG, and Anderson RG (1993) Mis-assembly of clathrin lattices on endosomes reveals a regulatory switch for coated pit formation. *J Cell Biol* **123**:1107–1117.
- Yan Z, Chi P, Bibb JA, Ryan TA, and Greengard P (2002) Roscovitine: a novel regulator of P/Q-type calcium channels and transmitter release in central neurons. *J Physiol* **540**:761–770.
- Zheng J, Cahill SM, Lemmons MA, Fushman D, Schlessinger J, Cowburn D, and Lemmon MA (1996) Identification of the binding site for acidic phospholipids on the PH domains of dynamain: implications for stimulation of GTPase activity. *J Mol Biol* **255**:14–21.

**Address correspondence to:** Dr. Phillip J. Robinson, Cell Signaling Unit, Children's Medical Research Institute, Locked Bag 23, Wentworthville, Sydney, NSW 2145, Australia. E-mail: [probinson@cmri.com.au](mailto:probinson@cmri.com.au)